

THE REPEATING FAST RADIO BURST FRB 121102: MULTI-WAVELENGTH OBSERVATIONS AND ADDITIONAL BURSTS

P. SCHOLZ¹, L. G. SPITLER², J. W. T. HESSELS^{3,4}, S. CHATTERJEE⁵, J. M. CORDES⁵, V. M. KASPI¹, R. S. WHARTON⁵, C. G. BASSA³, S. BOGDANOV⁷, F. CAMILO^{7,8}, F. CRAWFORD⁹, J. DENEVA¹⁰, J. VAN LEEUWEN^{3,4}, R. LYNCH¹¹, E. C. MADSEN¹, M. A. MC LAUGHLIN¹², M. MICKALIGER⁶, E. PARENT¹, C. PATEL¹, S. M. RANSOM¹³, A. SEYMOUR¹⁴, I. H. STAIRS^{15,1}, B. W. STAPPERS⁶, & S. P. TENDULKAR¹

Draft version January 29, 2022

ABSTRACT

We report on radio and X-ray observations of the only known repeating Fast Radio Burst (FRB) source, FRB 121102. We have detected six additional radio bursts from this source: five with the Green Bank Telescope at 2 GHz, and one at 1.4 GHz at the Arecibo Observatory for a total of 17 bursts from this source. All have dispersion measures consistent with a single value ($\sim 559 \text{ pc cm}^{-3}$) that is three times the predicted maximum Galactic value. The 2-GHz bursts have highly variable spectra like those at 1.4 GHz, indicating that the frequency structure seen across the individual 1.4 and 2-GHz bandpasses is part of a wideband process. X-ray observations of the FRB 121102 field with the *Swift* and *Chandra* observatories show at least one possible counterpart; however, the probability of chance superposition is high. A radio imaging observation of the field with the Jansky Very Large Array at 1.6 GHz yields a 5σ upper limit of 0.3 mJy on any point-source continuum emission. This upper limit, combined with archival WISE 22- μm and IPHAS H α surveys, rules out the presence of an intervening Galactic H II region. We update our estimate of the FRB detection rate in the PALFA survey to be $1.1_{-1.0}^{+3.7} \times 10^4 \text{ FRBs sky}^{-1} \text{ day}^{-1}$ (95% confidence) for peak flux density at 1.4 GHz above 300 mJy. We find that the intrinsic widths of the 12 FRB 121102 bursts from Arecibo are, on average, significantly longer than the intrinsic widths of the 13 single-component FRBs detected with the Parkes telescope.

Subject headings: pulsars: general — stars: neutron — radio continuum: general — X-rays: general

1. INTRODUCTION

Fast Radio Bursts (FRBs) are an emerging class of astrophysical transients whose physical origin is still a mystery. They are relatively bright (peak fluxes $\sim 0.5 - 1 \text{ Jy}$ at 1.4 GHz), millisecond-duration radio bursts with high dispersion measures (DMs $\gtrsim 300 \text{ pc cm}^{-3}$) that significantly exceed the maximum expected line-of-sight con-

tribution in the NE2001 model of Galactic electron density (Cordes & Lazio 2002), and are thus thought to be extragalactic in origin. The distances implied by their DMs, assuming that the excess dispersion is dominated by the intergalactic medium (IGM) and a modest contribution from the host galaxy, place them at cosmological redshifts (e.g., Thornton et al. 2013). Alternatively, if the majority of the DM comes from near the source, they could be located in galaxies at distances of tens to hundreds of megaparsecs (e.g., Masui et al. 2015).

With the exception of one FRB detected with the 305-m Arecibo telescope (Spitler et al. 2014) and one with the 110-m Robert C. Byrd Green Bank Telescope (GBT; Masui et al. 2015), all of the 17 currently known FRBs have been detected using the 64-m Parkes radio telescope (Lorimer et al. 2007; Thornton et al. 2013; Burke-Spolaor & Bannister 2014; Ravi et al. 2015; Petroff et al. 2015a; Champion et al. 2015; Keane et al. 2016). While Arecibo and GBT provide significantly higher raw sensitivity ($\sim 3-10$ times greater than Parkes), the comparatively large field of view of the Parkes telescope, combined with the survey speed of its 13-beam receiver, has proven to be a big advantage for blind FRB searches. Petroff et al. (2016), hereafter FRBCAT, present an online catalog of the known FRBs and their properties¹⁶.

The first FRB detected at a telescope other than Parkes was found in data from the PALFA pulsar and fast transient survey (Cordes et al. 2006; Lazarus et al. 2015), which uses the 7-pixel Arecibo L-Band Feed Array (ALFA) receiver system. The burst, FRB 121102, was discovered in a survey pointing towards the Galac-

¹ Dept. of Physics and McGill Space Institute, McGill Univ., Montreal, QC H3A 2T8, Canada; pscholz@physics.mcgill.ca

² Max-Planck-Institut für Radioastronomie, Auf dem Hügel 69, 53121 Bonn, Germany

³ ASTRON, the Netherlands Institute for Radio Astronomy, Postbus 2, 7990 AA Dwingeloo, The Netherlands; J.W.T.Hessels@uva.nl

⁴ Anton Pannekoek Institute for Astronomy, Univ. of Amsterdam, Science Park 904, 1098 XH Amsterdam, The Netherlands

⁵ Dept. of Astronomy and Cornell Center for Astrophysics and Planetary Science, Cornell Univ., Ithaca, NY 14853, USA

⁶ Jodrell Bank Centre for Astrophysics, Univ. of Manchester, Manchester, M13 9PL, UK

⁷ Columbia Astrophysics Laboratory, Columbia Univ., New York, NY 10027, USA

⁸ SKA South Africa, Pinelands, 7405, South Africa

⁹ Dept. of Physics and Astronomy, Franklin and Marshall College, Lancaster, PA 17604-3003, USA

¹⁰ National Research Council, resident at the Naval Research Laboratory, 4555 Overlook Avenue SW, Washington DC 20375, USA

¹¹ National Radio Astronomy Observatory, PO Box 2, Green Bank, WV 24944, USA

¹² Dept. of Physics and Astronomy, West Virginia Univ., Morgantown, WV 26506, USA

¹³ National Radio Astronomy Observatory, Charlottesville, VA 22903, USA

¹⁴ Arecibo Observatory, HC3 Box 53995, Arecibo, PR 00612, USA

¹⁵ Dept. of Physics and Astronomy, Univ. of British Columbia, Vancouver, BC V6T 1Z1, Canada

¹⁶ <http://www.astronomy.swin.edu.au/pulsar/frbcat/>

tic anti-center and in the plane: $l \sim 175^\circ$, $b \sim -0.2^\circ$ (Spitler et al. 2014). The DM was measured to be $557 \pm 2 \text{ pc cm}^{-3}$, three times in excess of the Galactic line-of-sight DM predicted by the NE2001 model (Cordes & Lazio 2002).

Spitler et al. (2016) performed follow-up observations with the Arecibo telescope in 2013 December and 2015 May–June using a grid of ALFA pointings around the position of the original FRB 121102 burst. In three separate 2015 May–June observations, 10 additional bursts were detected at a DM and position consistent with the original detection (Spitler et al. 2016).

Thus far, no Parkes or GBT-detected FRB has been observed to repeat, despite dozens of hours of follow-up observations in some cases (Petroff et al. 2015b; Masui et al. 2015). The cosmological distances sometimes assumed for these events, along with their apparent non-repeatability, has led to many theories of FRB origins that involve cataclysmic events. Examples include the merger of neutron stars or white dwarfs (Kashiyama et al. 2013), or the collapse of a fast-spinning and anomalously massive neutron star into a black hole (Falcke & Rezzolla 2014). The discovery of a repeating FRB shows that, for at least a subset of the FRB population, the origin of such bursts cannot be from a cataclysmic event. Rather, they must be due to a repeating phenomenon such as giant pulses from neutron stars (Cordes & Wasserman 2016; Pen & Connor 2015). The lack of observed repetition from the Parkes-discovered sources could, in principle, be due to the Parkes telescope’s lower sensitivity compared to that of the Arecibo telescope. If so, it is possible that all FRBs have a common physical origin, but that the observed population of bursts is strongly biased by limited sensitivity.

In stark contrast to the origin implied by the repeating FRB 121102, Keane et al. (2016) have recently claimed the detection of a fading radio afterglow associated with the Parkes-discovered FRB 150418 at a redshift of 0.5. Unlike FRB 121102, this discovery suggests that some FRBs may indeed originate from cataclysmic events, as the merger of neutron stars is the preferred explanation. However, Williams & Berger (2016) and Vedantham et al. (2016) have challenged the afterglow association, suggesting that it may instead be unrelated flaring from an active galactic nucleus (AGN). If this conclusion is supported by continued monitoring of the FRB 150418 field, then there is no need yet to postulate two separate types of FRB progenitors.

The detected bursts from FRB 121102 have several peculiar properties when compared with the pulses typically seen from canonical radio pulsars; this undoubtedly provides important clues to their physical origin. First, they appear to arrive clustered in time: of the 10 bursts presented by Spitler et al. (2016), six arrived within a ~ 10 -min period, despite having a total of ~ 4 hr of on-source time in the 2013 December and 2015 May–June follow-up campaigns. The bursts also displayed unusual and highly variable spectral properties: some bursts brighten significantly towards the highest observed frequencies, whereas others become much brighter towards lower frequencies. Spitler et al. (2016) characterized this behavior with power-law flux density models ($S_\nu \propto \nu^\alpha$, where S_ν is the flux density at frequency ν) where the

observed spectral index varied between $\alpha \sim -10$ to $+14$. Even more peculiar is that at least two of the bursts are obviously poorly described by a power-law model and appear to have spectra that peak within the 322 MHz-wide band of ALFA. Lastly, the detected bursts show no obvious signs of scintillation or scattering, both of which could provide important insights into the distance and source environment.

In this paper, we present further follow-up observations of FRB 121102 and the surrounding field using the *Swift* and *Chandra* X-ray telescopes, the Karl G. Jansky Very Large Array (VLA), and Arecibo, Green Bank, Lovell and Effelsberg radio telescopes. In Section 2 we describe the observations taken and the resulting datasets. In Section 3 we outline our analysis of bursts detected in Arecibo and GBT observations. We present images of the field around FRB 121102 from our VLA, *Swift* and *Chandra* observations, as well as archival optical and high-energy observations in Section 4. We revisit the question of whether the source could be Galactic in Section 5. In Section 6, we present an updated FRB rate from the PALFA survey. In Section 7 we discuss the implications of a repeating FRB as well as the properties of our bursts in the context of other FRB detections.

2. OBSERVATIONS

Following the Arecibo discovery of repeat bursts from FRB 121102 (Spitler et al. 2016), we performed additional follow-up observations using a variety of telescopes. Unless otherwise noted, each telescope was pointed at the average position of the 2015 May–June detections from Spitler et al. (2016): i.e. RA= $05^\circ 31' 58''$ and Dec= $+33^\circ 08' 04''$. Spitler et al. (2016) quote a conservative uncertainty region of $6'$ in diameter, approximately twice the full-width at half maximum (FWHM) of an ALFA beam at 1.4 GHz. Table 1 summarizes the observing set-ups used and Table 2 lists all radio observations of FRB 121102, including the ALFA discovery and follow-up observations presented by Spitler et al. (2016). Figure 1 shows a timeline of the radio and X-ray observations that we performed.

2.1. Arecibo Telescope

We observed FRB 121102 with the 305-m William E. Gordon Telescope at the Arecibo Observatory (AO) using the single-pixel L-Wide receiver (1100 – 1750 MHz) and the Puerto-Rican Ultimate Pulsar Processing Instrument (PUPPI) backend. We used PUPPI’s coherent filterbank mode, in which each of seven 100-MHz bands are sampled with $10.24\text{-}\mu\text{s}$ time resolution and 512 spectral channels. Each of the spectral channels was coherently dedispersed at $\text{DM} = 557.0 \text{ pc cm}^{-3}$. As such, the recorded signals do not suffer significantly from intra-channel dispersive smearing (unlike the ALFA observations presented in Spitler et al. 2016, which use the Mock spectrometers¹⁷ and incoherent dedispersion). Observing sessions ranged from roughly 1 – 2 hr in length (FRB 121102 is only visible to Arecibo for ~ 2 hr per transit), and typically we observed a 2-min scan on a test pulsar, followed by a single long pointing at the best known position of FRB 121102. All scans were preceded by a 60-s calibration observation of a pulsed noise

¹⁷ <http://www.naic.edu/astro/mock.shtml>

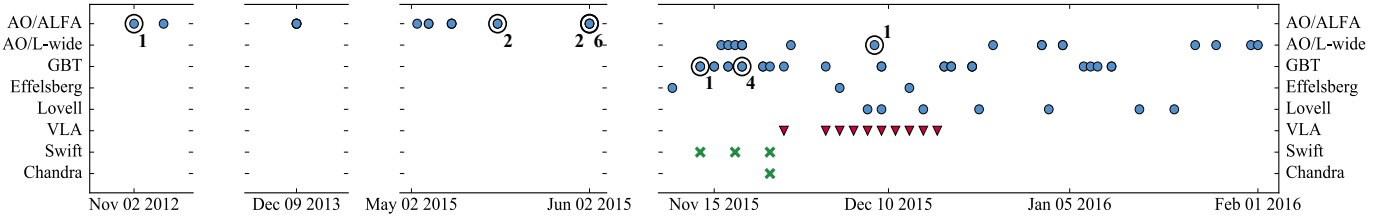


Figure 1. Timeline of radio and X-ray observations of FRB 121102 from discovery in 2012 November to 2016 January. Each row represents a set of observations from a given telescope (and receiver in the case of Arecibo observations). Blue circles represent single-dish radio observations, red triangles denote radio interferometer observations and green crosses are X-ray observations. Observations with bursts are encircled and marked with the numbers of bursts discovered. Note that bursts were discovered on 2015 June 2 in two separate observations.

Table 1
Summary of Radio Telescope Observations

Telescope	Receiver	Gain (K/Jy)	T_{sys} (K)	Bandwidth (MHz)	Central Frequency (MHz)	Beam FWHM (')	Total Time on-source (hr)
Arecibo	ALFA ^a	8.5	30	322	1375	3.4	4.4
Arecibo	L-Wide ^b	10	30	700 ^g	1430	3.1	11.4
GBT	S-band ^c	2.0	20	800 ^g	2000	5.8	15.3
GBT	820 MHz ^c	2.0	25	200	820	15	7.4
Effelsberg	S60mm ^d	1.55	27	500	4850	2.4	9.7
Lovell	L-band	0.9	27	400	1532	12	14.0
Jansky VLA	L-band ^e	2.15	35	2 × 128	1436, 1800	0.5–0.75 ^f	10.0

^a http://www.naic.edu/alfa/gen_info/info_obs.shtml

^b <http://www.naic.edu/~astro/RXstatus/Lwide/Lwide.shtml>

^c <https://science.nrao.edu/facilities/gbt/proposing/GBTpg.pdf>

^d https://eff100mwiki.mpifr-bonn.mpg.de/doku.php?id=information_for_astronomers:rx:s60mm

^e <https://science.nrao.edu/facilities/vla/docs/manuals/oss2015B>

^f For synthesized beam

^g RFI filters reduce the usable bandwidth to ∼ 600 MHz

diode. On a few occasions we observed alternate pointing positions consistent with the 2015 May/June detection beams reported by Spitler et al. (2016) – i.e. positions offset by a few arcminutes with respect to the average position quoted above. The details of each session are given in Table 2.

To search for bursts from FRB 121102, we used standard tools from the PRESTO software suite (Ransom 2001)¹⁸. We first identified RFI-contaminated frequency channels and time blocks using `rfifind`. Those channels and blocks were masked in subsequent analysis. We produced dedispersed time series in the DM range 487–627 pc cm⁻³ with a step size of 1 pc cm⁻³. For each time series, we searched for significant single-pulse signals using `single_pulse_search.py`. One bright burst was found in an observation on 2015 December 8 (see Section 3 and Figure 2). Remaining RFI in the data complicates the search for weaker bursts. More sophisticated RFI excision could lead to the identification of additional, weak bursts in these data sets. A deeper search of the data can also be guided by the possible future determination of an underlying periodicity. Currently, the Arecibo PUPPI burst searches have an approximate 12 σ threshold.

2.2. Green Bank Telescope

We observed FRB 121102 with the 110-m Robert C. Byrd Green Bank Telescope (GBT) using the Green Bank Ultimate Pulsar Processing Instrument (GUPPI)

backend and the 820-MHz and 2-GHz receivers. The 820-MHz observations used a 200-MHz bandwidth and recorded spectra every 20.48 μ s. The 2-GHz observations have 800 MHz of nominal bandwidth (RFI filters reduce the usable bandwidth to about 600 MHz) and the spectra were recorded every 10.24 μ s. Note that the GBT beam has a FWHM of ∼ 6' at 2 GHz and thus comfortably encompasses the conservative positional uncertainty of FRB 121102 despite the higher observing frequency. In each case, the data were coherently dedispersed at the nominal DM of FRB 121102 and 512 spectral channels were recorded with full Stokes parameters. During a single observing session, we observed FRB 121102 typically for 50 min using each receiver. We also observed a pulsed noise diode at the start of each scan for use in absolute flux calibration. A detailed description of each session is given in Table 2.

Using standard PRESTO tools, dedispersed time series were generated at DMs in the range 527–587 pc cm⁻³ with a step size of 0.1 pc cm⁻³ at 2 GHz and 0.05 pc cm⁻³ at 820 MHz. They were then searched for single-pulse signals in the time domain. One burst was found in a 2 GHz observation on 2015 November 13 and four additional bursts were found in 2 GHz observations on 2015 November 19 (see Section 3 and Figure 2). FRB 121102 was not detected in any 820 MHz GBT observations.

2.3. Lovell Telescope

We observed the position of FRB 121102 with the Lovell Telescope at the Jodrell Bank Observatory on

¹⁸ <http://www.cv.nrao.edu/~sransom/presto/>

seven separate epochs (see Table 2) for a total of 14 hr. Spectra were recorded with a total bandwidth of 400 MHz over 800 channels with a center frequency of 1532 MHz, at a sampling time of 256 μ s. Unlike for the Arecibo and GBT observations, the spectral channels were not coherently dedispersed. The data were RFI-filtered using a median absolute deviation algorithm before applying a channel mask, which results in typically $\sim 20\%$ of the band being removed. The cleaned data were dedispersed at DMs in the range 527–587 pc cm $^{-3}$ with a step size of 0.5 pc cm $^{-3}$. Each DM was then searched for single-pulse signals using the SIGPROC `seek` command. No candidates above a threshold of 7σ were detected.

2.4. Effelsberg Telescope

We observed the position of FRB 121102 with the Effelsberg 100-m Radio Telescope using the S60mm receiver, which covers the frequency range 4600–5100 MHz, and the Pulsar Fast-Fourier-Transform Spectrometer (PFITS) search backend. The FWHM of the Effelsberg telescope at 5 GHz is 2.4'. As such, the high-frequency Effelsberg observations covered only the central region of the positional error box given in Spitler et al. (2016). The PFITS spectrometers generate total intensity spectra with a frequency resolution of 3.90625 MHz and time resolution of 65.536 μ s. Dedispersed time series were generated at DMs in the range 408–712 pc cm $^{-3}$ with a step size of 8 pc cm $^{-3}$ and searched for single-pulse signals using standard PRESTO tools, as above. No bursts above a threshold of 8σ were found.

2.5. Jansky Very Large Array

We observed the FRB 121102 field at 1.6 GHz for 10 hr with the Karl G. Jansky Very Large Array (VLA) in D-configuration (Project Code: VLA/15B-378) to better localize the FRB position and to set limits on the distribution of free electrons along the line of sight (see Section 5). The 10 hr were split into ten 1-hr observations occurring every few days from 2015 November 25 to 2015 December 17. Each 1-hr observation consisted of a preliminary scan of the flux calibrator J0542+4951 (3C147) followed by three 14-min scans on the FRB field bracketed by 100-s scans on the phase calibrator J0555+3948.

Data were collected in the shared-risk fast-sample correlator mode (see, e.g., Law et al. 2015) with visibilities recorded every 5 ms. The bandwidth available in this mode is currently limited by the correlator throughput to 256 MHz, which we split into two 128-MHz subbands. The subbands were centered on frequencies of 1435.5 MHz and 1799.5 MHz to avoid known RFI sources. By observing in the fast-sample mode, we are able to produce channelized time series data for any synthesized beam within the $\sim 0.5^\circ$ primary field of view (28' across) in addition to the standard interferometric visibilities. If a pulse is detected in the time-series data, it will localize FRB 121102 to within one synthesized beam (about 30'' – 45'' in D-configuration at 1.6 GHz, depending on hour angle coverage and visibility weighting in the image). The results of the time-domain burst search will be presented in a subsequent paper (Wharton et al., in prep). The analysis of these data is described below in Section 4.1. Here we present only the imaging results.

Table 2 Details of Radio Telescope Observations

Date	Start Time (UTC)	Telescope/Receiver	Obs. Length, t_{obs} (s)	No. Bursts
2012-11-02	06:38:13	AO/ALFA	181	1
2012-11-04	06:28:43	AO/ALFA	181	0
2013-12-09	04:09:52	AO/ALFA	2702	0
2013-12-09	05:14:32	AO/ALFA	1830	0
2013-12-09	04:55:19	AO/ALFA	970	0
2015-05-03	18:55:48	AO/ALFA	1502	0
2015-05-05	18:29:07	AO/ALFA	1002	0
2015-05-05	19:39:15	AO/ALFA	1002	0
2015-05-09	18:10:48	AO/ALFA	1002	0
2015-05-09	19:20:56	AO/ALFA	1002	0
2015-05-09	19:38:12	AO/ALFA	425	0
2015-05-17	17:45:38	AO/ALFA	1002	2
2015-05-17	18:58:07	AO/ALFA	1002	0
2015-06-02	16:38:47	AO/ALFA	1002	2
2015-06-02	17:48:52	AO/ALFA	1002	6
2015-06-02	18:09:18	AO/ALFA	300	0
2015-11-09	22:36:47	Effelsberg	9894	0
2015-11-13	06:38:51	GBT/820 MHz	3000	0
2015-11-16	05:24:09	AO/L-wide	5753	0
2015-11-13	07:42:09	GBT/S-band	3000	1
2015-11-15	02:55:50	GBT/S-band	3000	0
2015-11-15	03:57:08	GBT/820 MHz	3000	0
2015-11-17	03:24:33	GBT/S-band	3000	0
2015-11-17	04:34:40	GBT/820 MHz	3000	0
2015-11-17	05:21:37	AO/L-wide	6747	0
2015-11-18	05:23:14	AO/L-wide	6421	0
2015-11-19	05:27:12	AO/L-wide	3000	0
2015-11-19	06:19:36	AO/L-wide	1300	0
2015-11-19	06:43:46	AO/L-wide	971	0
2015-11-19	10:14:57	GBT/S-band	3000	4
2015-11-19	11:16:32	GBT/820 MHz	1653	0
2015-11-22	08:45:23	GBT/S-band	3000	0
2015-11-22	09:47:15	GBT/820 MHz	2543	0
2015-11-23	11:42:40	GBT/S-band	5357	0
2015-11-25	03:25:29	VLA	3585	-
2015-11-25	10:48:05	GBT/S-band	5264	0
2015-11-26	05:18:03	AO/L-wide	2705	0
2015-12-01	05:31:31	VLA	3590	-
2015-12-01	07:46:17	GBT/S-band	6480	0
2015-12-03	02:53:57	VLA	3589	-
2015-12-03	03:42:14	Effelsberg	10800	0
2015-12-05	04:45:44	VLA	3589	-
2015-12-07	04:37:50	VLA	3589	-
2015-12-07	21:36:17	Lovell	7229	0
2015-12-08	04:43:24	AO/L-wide	3625	1
2015-12-09	00:01:52	Lovell	7209	0
2015-12-09	08:11:46	GBT/S-band	3141	0
2015-12-09	09:29:25	VLA	3590	-
2015-12-09	09:40:28	GBT/820 MHz	3106	0
2015-12-11	09:22:27	VLA	3590	-
2015-12-13	00:38:29	Effelsberg	14400	0
2015-12-13	09:13:07	VLA	3589	-
2015-12-15	04:01:29	Lovell	7141	0
2015-12-15	09:06:16	VLA	3590	-
2015-12-17	08:57:51	VLA	3589	-
2015-12-18	08:55:38	GBT/S-band	3600	0
2015-12-18	10:08:41	GBT/820 MHz	2216	0
2015-12-19	00:05:44	GBT/S-band	3600	0
2015-12-19	01:19:43	GBT/820 MHz	1510	0
2015-12-22	00:11:13	GBT/S-band	830	0
2015-12-22	00:28:24	GBT/S-band	2024	0
2015-12-22	01:15:13	GBT/820 MHz	2688	0
2015-12-23	04:55:57	Lovell	7225	0
2015-12-25	04:19:06	AO/L-wide	1534	0
2016-01-01	02:23:17	AO/L-wide	5858	0
2016-01-01	04:15:37	AO/L-wide	46	0
2016-01-02	01:16:52	Lovell	7207	0
2016-01-04	03:09:06	AO/L-wide	1700	0
2016-01-04	03:40:06	AO/L-wide	1200	0
2016-01-07	23:14:07	GBT/S-band	3300	0
2016-01-08	00:35:28	GBT/820 MHz	1513	0
2016-01-09	22:16:19	GBT/S-band	3300	0
2016-01-11	00:57:08	GBT/S-band	3300	0
2016-01-11	02:06:44	GBT/820 MHz	2264	0
2016-01-15	00:54:35	Lovell	7208	0
2016-01-20	02:43:36	Lovell	7215	0
2016-01-23	00:56:47	AO/L-wide	6485	0
2016-01-26	00:58:17	AO/L-wide	6058	0
2016-01-31	00:28:44	AO/L-wide	6362	0
2016-02-01	00:30:20	AO/L-wide	6284	0

2.6. *Swift & Chandra*

We performed observations with the *Swift* X-ray Telescope (Burrows et al. 2005), which is sensitive to X-rays between 0.3–10 keV, on 2015 November 13, 18, and 23 (Obs IDs 00034162001, 00034162002, 00034162003). The observations were performed in Photon Counting (PC) mode, which has a time resolution of 2.5 s and had exposure times of 5 ks, 1 ks and 4 ks, respectively. We downloaded the Level 1 data from the HEASARC archive and ran the standard data reduction script `xrtpipeline` using HEASOFT 6.17 and the *Swift* 20150721 CALDB.

On 2015 November 23, *Chandra* X-ray Observatory observations were performed using ACIS-S in Full Frame mode, which provides a time resolution of 3 s and sensitivity to X-rays between 0.1–10 keV (Obs ID 18717). The total exposure time was 39.5 ks. The data were processed with standard tools from CIAO 4.7 with *Chandra* CALDB 4.6.7. Note that we also performed a simultaneous 1.5-hr GBT observation during the *Chandra* session (see Section 2.2) but detected no radio bursts in those data.

For both the *Swift* and *Chandra* observations, we corrected the event arrival times to the solar system barycenter using the average FRB 121102 position from Spitler et al. (2016).

The analysis of these data is described below in Section 4.2.

3. REPEATING RADIO BURSTS

In addition to the 11 bursts detected using the Arecibo ALFA receiver and reported by Spitler et al. (2014, 2016), we have detected a further six bursts: five in GBT GUPPI observations with the S-band receiver and one in an Arecibo PUPPI observation using the L-wide receiver (see Table 2). All five GBT bursts were found at 2 GHz; no bursts were found in the GBT 820-MHz observations. Further, four of them were found within ~ 20 min on 2015 November 19.

In Figure 2 we show each burst as a function of observing frequency and time. Each burst has been dedispersed to a DM of 559 pc cm^{-3} . The data have been corrected for the receiver bandpass, which was estimated from the average of the raw data samples of each channel. That average bandpass was then median filtered with a width of 20 channels to remove the effects of narrow-band RFI. Frequency channels identified as containing RFI by PRESTO’s `rfifind` were masked. The data were down-sampled to 32 frequency channels and a time resolution of 1.3 ms. The top panel for each burst plot shows the frequency-summed time series and the side panel shows the spectrum summed over a 10-ms window centered on the burst peak. We continue the burst numbering convention used in Spitler et al. (2016) whereby bursts are numbered sequentially in order of detection. The first GBT burst is thus designated “burst 12”, as the bursts presented in Spitler et al. (2016) were numbered from 1–11. We choose this approach in order to avoid conflict with the burst identifiers used in Spitler et al. (2016), but caution that there may be weaker pulses in these data which can be identified by future, deeper analyses (e.g. if an underlying source periodicity is found, then this can guide the search for weaker pulses).

In Figure 3 we highlight frequency-dependent profile

evolution in bursts 8, 10 and 13. As observed in Spitler et al. (2016), the ALFA-detected bursts 8 and 10 show evidence for double-peaked profiles. Here we show that the double-peak behavior is apparent at high frequencies, but the two peaks seem to blend into a single peak at lower frequencies. For burst 13, which is detected in only the top three subbands shown in Figure 3, the burst in the 1.8–2 GHz subband is wider than in the two higher frequency subbands, causing a bias in the DM measurement (see below).

3.1. Temporal and Flux Properties

For each burst we measured the peak flux, fluence and burst width (FWHM). Before measuring these properties we normalized each burst time series using the radiometer equation where the noise level is given by

$$\frac{T_{\text{sys}}}{G\sqrt{2Bt_{\text{int}}}}, \quad (1)$$

where T_{sys} is the system temperature of the receiver, 20 K for GBT 2-GHz observations and 30 K for Arecibo L-wide; G is the gain of the telescope, 2 K/Jy for GBT and 10 K/Jy for Arecibo; B is the observing bandwidth; and t_{int} is the width of a time-series bin. The peak flux is the highest 1.3 ms-wide bin in this normalized time series. The fluence is the sum of this normalized time series. To measure the width we fit the burst with a Gaussian model. The peak time is the best-fit mean in the Gaussian model.

In Table 3 we show the above measured properties for each burst. The GUPPI bursts have peak flux densities in the range $0.02 - 0.09 \text{ Jy}$ at 2 GHz assuming the bursts are detected on axis. These are similar to the range of peak flux densities found for the ALFA-detected bursts presented by Spitler et al. (2016), $0.02 - 0.3 \text{ Jy}$. The PUPPI-detected burst had a peak flux density of 0.03 Jy , again assuming a perfectly on-axis detection, similar to the faintest bursts seen by Spitler et al. (2016).

3.2. Dispersion Properties

We measured the DM of each burst except burst 15, which was detected over too narrow a frequency range to make a reliable DM measurement. For each burst, time series were generated in subbands by averaging over blocks of frequency channels. The number of subbands depended on the signal-to-noise ratio (S/N) of the burst, and subbands with too little signal or too contaminated by RFI were excluded. Times of arrival (TOAs) for each frequency subband were calculated using a Gaussian template. The width of the Gaussian template was chosen to match the burst width measured from the whole band, as described above. TEMPO2¹⁹ (Hobbs et al. 2006) was used to find the best-fit DM from the TOAs. The results are given in Table 3.

Several of these bursts (13 and 14) have formal DM measurements which are larger than the mean by a statistically significant margin. We argue that this reflects un-modeled frequency-dependent profile evolution (see Figure 3) and not a measurement of time-variable DM. Our simple Gaussian template assumes a constant burst shape and width across the band. If the burst shape

¹⁹ <http://www.atnf.csiro.au/research/pulsar/tempo2/>

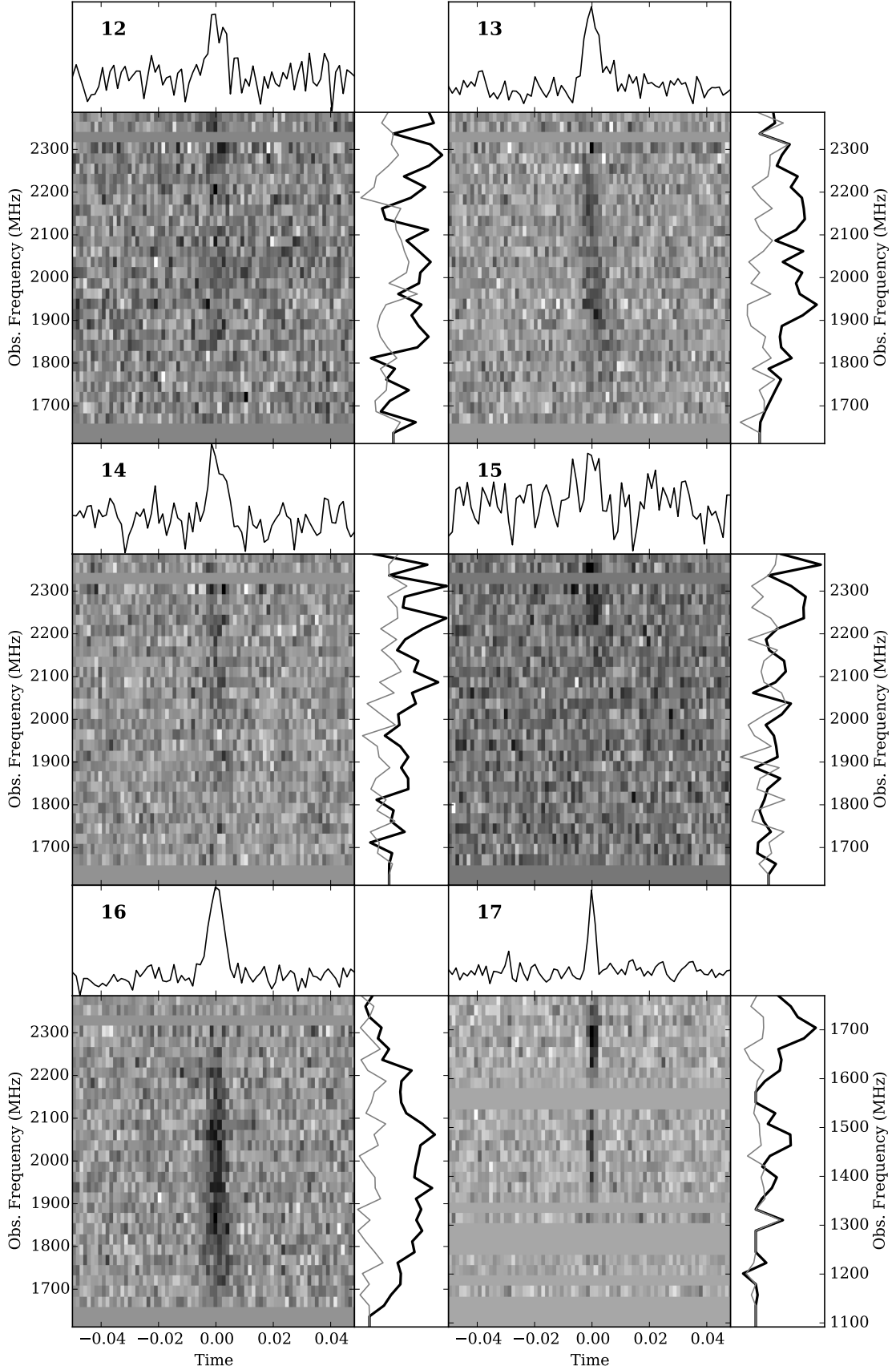


Figure 2. Dynamic spectra for each of the bursts detected in 2015 November and December using GUPPI (bursts 12 – 16) and PUPPI (burst 17) dedispersed at $DM=559 \text{ pc cm}^{-3}$. For each burst, total intensity is shown in grayscale, the top panels show the burst time series summed over frequency, and the side panels show bandpass-corrected burst spectra summed over a 10-ms window centered on the burst. The on-burst spectrum is shown as a black line and an off-burst spectrum is shown as a gray line to show the noise level. Note that some frequency channels are masked due to RFI.

varies across the band, then the TOA will shift to reflect the shift in the concentration of the flux density (Hassall et al. 2012).

We explored this in depth for burst 13, which has higher S/N than burst 14. The value of $565.1 \pm 1.8 \text{ pc cm}^{-3}$ quoted in Table 3 was calculated by dividing the full bandpass into eight subbands but only including the TOAs from the top five subbands in the fit (i.e. excluding data below 1900 MHz due to low S/N). If instead we include TOAs above $\sim 1700 \text{ MHz}$, the value drops to $560.0 \pm 1.2 \text{ pc cm}^{-3}$. Similarly, calculating TOAs for four subbands instead of eight and including only the TOAs above 1800 MHz gives a value of $569.2 \pm 1.8 \text{ pc cm}^{-3}$. The spread in these fitted values is larger than the formal uncertainties reported by TEMPO2 by a factor of ~ 3 . Clearly there are systematic effects in the burst profiles which are not accounted for by the TEMPO2 uncertainties.

Spitler et al. (2016) estimated the systematic uncertainty for bursts 1–11 by calculating the ΔDM that results in a DM delay across the band equal to half the burst width. This has been calculated for each GUPPI and PUPPI-detected burst and is the second uncertainty value given in Table 3. Adding the systematic uncertainties to the statistical uncertainties brings the DMs into agreement at the level of 1.5σ . Thus, there is currently no strong evidence for variations in the DM between bursts. The weighted average of the 15 bursts with measured DMs, excluding bursts 13 and 14 due to the above-mentioned profile variations, is $558 \pm 0.8 \text{ pc cm}^{-3}$.

Additionally, we measured the frequency index of the DM delay, i.e. $\Delta t_{\text{DM}} \propto \nu^{-\xi}$, for the brightest of the GUPPI bursts (burst 16). We expect $\xi = 2$ for the propagation of radio waves through a cold, ionized plasma. The consistency of the observed frequency sweep of FRBs with ν^{-2} has been used to argue their astrophysical origins, as it would be highly unlikely that RFI would mimic the dependence so exactly²⁰. The DM index was measured using a least-squares fitting code, which is described in detail by Spitler et al. (2016). The measured index for burst 16 is -1.997 ± 0.015 , consistent with -2 . Although the PUPPI-detected burst (burst 17) is also seen at high S/N, a large fraction of the band is masked due to RFI, making estimating a dispersion index difficult. The DM index has also been measured for both the discovery burst from FRB 121102 (Spitler et al. 2014), as well as the brightest of the bursts reported by Spitler et al. (2016), and all are consistent with -2 .

3.3. Spectral Properties

In Figure 2, we show the spectrum of each burst as a solid black line in the right panel of each burst sub-figure. The gray lines show the spectrum of the noise extracted from an off-pulse region that is the same width as the on-pulse region (a 10-ms time window). Due to low S/N, it is difficult to say anything about the GUPPI-detected burst spectra except for the brightest bursts (bursts 13 and 16). Burst 17, the PUPPI-detected burst, is also seen at high significance, but much of the band is cor-

rupted by RFI. Because of this, we do not attempt to fit any models to the spectra, and only describe them qualitatively here. Both bursts 13 and 16 have bandwidths of $\sim 600 \text{ MHz}$ and drop off in S/N at the edge of the 1.6–2.4 GHz band. It is clear that, as with the ALFA-detected bursts at 1.4 GHz (Spitler et al. 2016), the bursts detected at 2 GHz are not well described by a broadband power-law spectrum and that spectrum varies from burst to burst.

3.4. Polarization Properties

Each GUPPI and PUPPI-detected burst was extracted in the PSRFITS format using `dspsr`²¹, retaining all four Stokes parameters and the native time and frequency resolution of the raw data. These single pulses were calibrated with PSRCHIVE tools using the pulsed noise diode and the quasar J1442+0958 as a standard flux reference. No linear or circular polarization was detected. We searched for Faraday rotation using the PSRCHIVE²² `rmfit` routine in the range $\text{RM} \leq |20000| \text{ rad m}^{-2}$ but no significant RM was found. It should be noted that most of the GBT pulses are in a relatively low S/N regime, and a small degree of intrinsic polarization cannot be ruled out.

3.5. Periodicity Search

In Spitler et al. (2016), we searched for an underlying periodicity in the burst arrival times by attempting to fit a greatest common denominator to the differences in time between the 8 bursts that arrived on 2015 June 2 (bursts 4–11), but did not detect any statistically significant periodicities. Here, we apply an identical analysis to the four bursts detected on 2015 November 19 (bursts 13–16) and found that it was not possible to find a precise periodicity that fit all of the bursts detected. An apparent candidate periodicity at $424 \pm 20 \text{ s}$ was found, due to the burst spacings of 414, 441, and 416 seconds, but there were no significant periodicity candidates at shorter periods. As we concluded from the ALFA-detected bursts, more detections are necessary to determine whether any persistent underlying periodicity to the bursts is present.

In addition, we conducted a search for a persistent periodicity on dedispersed Arecibo and GBT observations using a fast-folding algorithm (FFA)²³. Originally designed by Staelin (1969), this algorithm operates in the time domain and is designed to be particularly effective at finding long-period pulsars (Lorimer & Kramer 2005; Kondratiev et al. 2009). The FFA offers greater period resolution compared to the FFT and has the advantage of coherently summing all harmonics of a given period, while the number of harmonics summed in typical FFT searches such as those performed by conventional pulsar search software, like PRESTO, is restricted, typically to ≤ 16 . This makes the time-domain analysis more sensitive to low rotational-frequency signals with high harmonic content, which are often obscured by red noise (e.g. Lazarus et al. 2015).

Prior to searching for periodic signals, RFI excision routines were applied to the observations. Such routines include a narrow-band mask generated by `rfifind`,

²⁰ In fact, the ‘Perytons’ (Burke-Spolaor et al. 2011), which have been shown to originate from on-site RFI at the Parkes observatory (Petroff et al. 2015c), do not precisely follow the expected pulse delay with frequency.

²¹ <http://dspsr.sourceforge.net>

²² <http://psrchive.sourceforge.net>

²³ Adapted from <https://github.com/petigura/FFA>

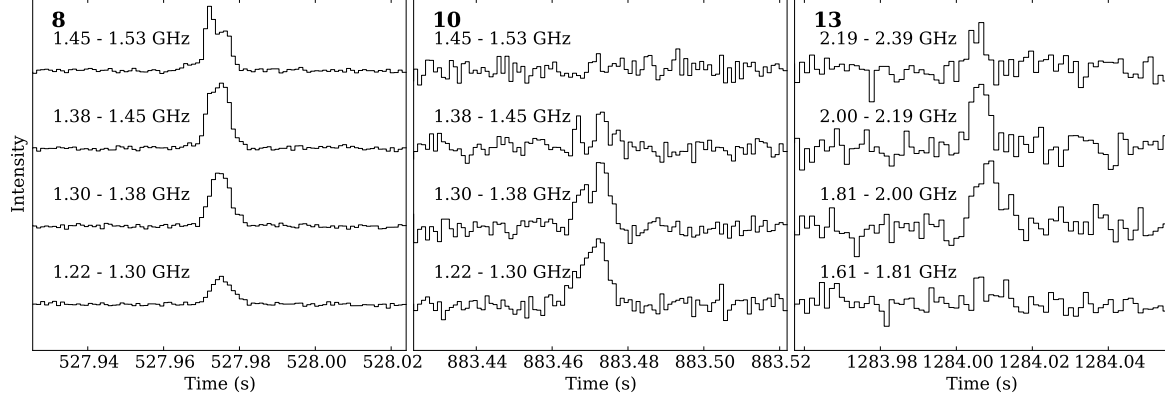


Figure 3. Burst time series plotted in four subbands for bursts 8, 10, and 13. The frequency range used for each subband is indicated above each time series. Frequency-dependent profile evolution is evident (see Section 3).

Table 3
Burst Properties

No.	Peak Time (MJD)	Peak Flux Density (Jy)	Fluence (Jy ms)	Gaussian FWHM (ms)	DM (pc cm ⁻³)
12	57339.356046005567	0.04	0.2	6.73 ± 1.12	$559.9 \pm 3.4 \pm 3.7$
13	57345.447691250090	0.06	0.4	6.10 ± 0.57	$565.1 \pm 1.8 \pm 3.4$
14	57345.452487925162	0.04	0.2	6.14 ± 1.00	$568.8 \pm 3.2 \pm 3.4$
15	57345.457595303807	0.02	0.08	4.30 ± 1.40	—
16	57345.462413106565	0.09	0.6	5.97 ± 0.35	$560.0 \pm 3.1 \pm 3.3$
17	57364.204632665605	0.03	0.09	2.50 ± 0.23	$558.6 \pm 0.3 \pm 1.4$

Note. — Bursts 12–16 were detected at 2 GHz at GBT and burst 17 was detected at 1.4 GHz at Arecibo. The errors quoted on DM are, in order, statistical and systematic. Burst peak times are corrected to the solar system barycenter and referenced to infinite frequency.

in which blocks flagged as containing RFI are replaced by constant data values matching the median bandpass. Bad time intervals were removed via PRESTO’s clipping algorithm (Ransom 2001) when samples in the $DM = 0 \text{ pc cm}^{-3}$ time series significantly exceeded the surrounding data samples. Moreover, a zero-DM filtering technique as described in Eatough et al. (2009) was also applied to the time series by removing the $DM = 0 \text{ pc cm}^{-3}$ signal from each frequency channel.

In this periodicity analysis, we searched periods ranging from 100 ms to 30 s. Below 100 ms, the number of required trials becomes prohibitive. Re-binning was performed such that the FFA search was sensitive to all possible pulse widths, ranging from duty cycles of 0.5% up to 50%.

For every ALFA, PUPPI, and GUPPI observation (see Table 2), candidates were generated by the FFA from the dedispersed, topocentric time series. Approximately 50 of the best candidates for each time series were folded using PRESTO’s `prepfold` and then inspected by eye. No promising periodic astrophysical sources were detected.

4. MULTI-WAVELENGTH FOLLOW-UP

4.1. VLA Imaging Analysis

The VLA data were processed with the Common Astronomy Software Applications (CASA; McMullin et al. 2007) package using the computing cluster at the Domenici Science Operations Center in Socorro, New Mexico. For the imaging analysis presented here, each observation was downsampled to increase the sampling time from 5 ms to 1 s. We then flagged the data and

performed standard complex gain calibration of the visibilities using our flux and phase calibrators. Using the seven brightest sources in the field, we ran three rounds of phase-only self-calibration followed by one round of amplitude self-calibration.

The flagged and calibrated data were imaged using CLEAN deconvolution (Schwab 1984). The two brightest sources in the field are located beyond the half-maximum point of the primary beam at 1.6 GHz. Since the primary beam width gets narrower with increasing frequency, these sources have very steep apparent spectral indices. To account for the spectral shape of these sources, we used the multi-frequency synthesis mode of the CASA CLEAN implementation (Rau & Cornwell 2011) and approximated the sky brightness as a first-order polynomial in frequency. As a result, we get both an image and a spectral index map for each of the ten single-epoch observations.

We combined all the single-epoch observations into one multi-epoch data set and performed a single round of amplitude-only self-calibration to correct any amplitude offsets in the visibility data between scans. The combined data were then imaged using the same procedure as the single-epoch imaging, producing by far the deepest radio continuum image to date for this field (see Figure 4a). No obvious new sources (see below) are seen in our FRB detection overlap region. The central $5' \times 5'$ region of the image has an RMS noise of $\sigma = 60 \mu\text{Jy beam}^{-1}$, with pixel values ranging from $-156 \mu\text{Jy beam}^{-1}$ to $209 \mu\text{Jy beam}^{-1}$. These results set a 5σ upper limit on the flux density of any point sources of $S_{\text{max}} = 0.3 \text{ mJy}$.

While no obvious new sources fall within the FWHM of the two ALFA beams of the re-detections, there are two previously identified sources within the 28 sq. arcmin conservative uncertainty region: J053210+3304 ($\alpha = 05^{\text{h}}32^{\text{m}}10^{\text{s}}08(3)$, $\delta = 33^{\circ}04'05.5(3)$) and J053153+3310 ($\alpha = 05^{\text{h}}31^{\text{m}}53^{\text{s}}91(2)$, $\delta = 33^{\circ}10'20.2(2)$). These sources were termed VLA1 and VLA2 by [Kulkarni et al. \(2015\)](#), who presented an analysis of archival data from the NRAO VLA Sky Survey (NVSS, [Condon et al. 1998](#)). J053210+3304 is consistent with a two-component AGN with the brighter component having a multi-epoch average flux density of $S_1 = 3.2 \pm 0.1$ mJy and spectral index $\alpha_{1.6} = -1.1 \pm 0.1$. J053153+3310 has a multi-epoch average flux density of $S_2 = 3.0 \pm 0.1$ mJy and spectral index of $\alpha_{1.6} = +1.7 \pm 0.1$. Imaging each of the ten epochs separately, we see that J053153+3310 is variable on timescales of a few days to a week, which is consistent with AGN variability (e.g., [Ofek et al. 2011](#)).

4.2. X-ray Data Analysis

We searched the *Chandra* image (Figure 4b) for sources using the CIAO tool `celldetect`. Table 4 shows the coordinates and number of counts in a circular extraction region with a 1'' radius ($\sim 90\%$ encircled power) for each detected source. There are five sources within the conservative 6' diameter uncertainty region shown as a solid circle in Figure 4b. Only one of these X-ray sources, CXOU J053156.7+330807 (No. 1 in Table 4 and Figure 4b) is within the 3.1' 1.4-GHz beam FWHM of our Arecibo PUPPI burst detection (see Section 2). We also searched the *Swift* observations using the HEASARC tool `ximage` and found no sources within the more conservative 6' uncertainty region.

We cannot assume that CXOU J053156.7+330807, or any of the other four sources in the more conservative uncertainty region, is a counterpart of FRB 121102. The *Chandra* image has seven detected sources within a 64 sq. arcmin field of view. Given this source density, the number of expected sources in any given 9 sq. arcmin (the FWHM area of an Arecibo 1.4-GHz beam) region is ~ 1 .

If we assume that CXOU J053156.7+330807 is associated with FRB 121102, and that the hydrogen column density, N_{H} , is correlated with DM according to the prescription of [He et al. \(2013\)](#), then the N_{H} toward the source would be $1.7_{-0.5}^{+0.7} \times 10^{22} \text{ cm}^{-2}$ (significantly higher than the predicted maximum Galactic N_{H} of $4.9 \times 10^{21} \text{ cm}^{-2}$, [Kalberla et al. 2005](#)). Assuming this N_{H} , the best-fit power-law index for a photoelectrically absorbed power-law model of the X-ray spectrum is $3.3 \pm 0.4_{-0.5}^{+0.7}$ and the 1–10 keV absorbed flux is $(9 \pm 3_{-0.5}^{+0.7}) \times 10^{-15} \text{ erg s}^{-1} \text{ cm}^{-2}$, where the first errors on the index and flux are statistical uncertainties and the second are systematic uncertainties from the spread in the N_{H} –DM relation of [He et al. \(2013\)](#). We note that these values are heavily dependent on the assumed N_{H} .

We also searched for variability during the 39.5-ks observation by making time series for each detected source with time resolutions of 3, 30, and 300 s. We then compared the predicted number of counts in each time bin with the average count rate. No significant deviations from a Poisson count rate were found for any of the sources.

4.3. Archival IR-Optical Observations

The field of FRB 121102 is in the anti-center region of the Galactic plane, and has been covered by several optical and infra-red surveys. We have examined archival images from the *Spitzer GLIMPSE 360* survey, the *2-Micron All-Sky Survey* (2MASS), and the *Second Palomar Observatory Sky Survey* (POSS II), among others. Due to the large radio beam in comparison to the angular resolution of optical and infra-red surveys, there are many sources within the positional uncertainty region of FRB 121102. It is thus impossible to identify a host galaxy, and we do not attempt to do so.

Alternatively, in order to further investigate the possibility of a Galactic origin, here we report on the two most constraining archival observations in terms of testing for the existence of a hypothetical Galactic H II region that could provide the excess dispersion of FRB 121102 compared with the maximum line-of-sight value expected from the NE2001 model.

The *Wide-field Infrared Survey Explorer* (WISE; [Wright et al. 2010](#)) space telescope covered the entire sky at multiple infrared bands (3.4, 4.6, 12, and 22 μm wavelengths). The 22- μm band images, with 12'' resolution and a sensitivity of 6 mJy, have been used by [Anderson et al. \(2014\)](#) to catalog Galactic H II regions with a high degree of completeness in conjunction with radio continuum imaging. We have extracted WISE 22- μm data in the region of interest from the NASA/IPAC Infrared Science Archive, as shown in Figure 4c, and find no sources within FRB 121102's positional uncertainty region, down to the sensitivity limit of the [Anderson et al. \(2014\)](#) survey.

However, several objects are present in the 3.4 (W1), 4.6 (W2) and 12 μm (W3) images. The ALLWISE catalog ([Cutri & et al. 2013](#)) lists 182 sources consistent with the best position of FRB 121102 (6' diameter), of which 23 have detections in the W1, W2 and W3 bands. [Nikutta et al. \(2014\)](#) find that the W2-W3 color is a reliable indicator to distinguish between stars and galaxies. They suggest using the criterion $\text{W2-W3} > 2$ for separating galaxies from stars. Using this indicator, we find that 9 of the 23 objects can be classified as being galaxies. We treat this value as a lower limit, as many WISE sources are not detected in the W3 band.

The *Isaac Newton Telescope Photometric H-Alpha Survey* (IPHAS; [Drew et al. 2005](#); [Barentsen et al. 2014](#)) provides optical survey images of the Galactic plane in our region of interest with a median seeing of 1.2'' and a broadband magnitude limit of ~ 20 or better at SDSS r' band, as well as narrow-band $\text{H}\alpha$ observations that are typically a magnitude brighter in limiting sensitivity. Since the field of interest is in the Galactic anti-center, the images are relatively uncrowded for the low Galactic latitude, and the $\text{H}\alpha$ image (Figure 4d) is devoid of any extended emission. No evidence is seen for a planetary nebula or a supernova remnant within the region.

In combination with our VLA 1.6-GHz (20-cm) observations, the non-detections at 22 μm and $\text{H}\alpha$ bands place a stringent limit on any Galactic H II regions or other sources that might contribute to FRB 121102's high DM, as discussed further in Section 5 (see also [Kulkarni et al. 2015](#)).

We can also look for optical and IR counterparts of

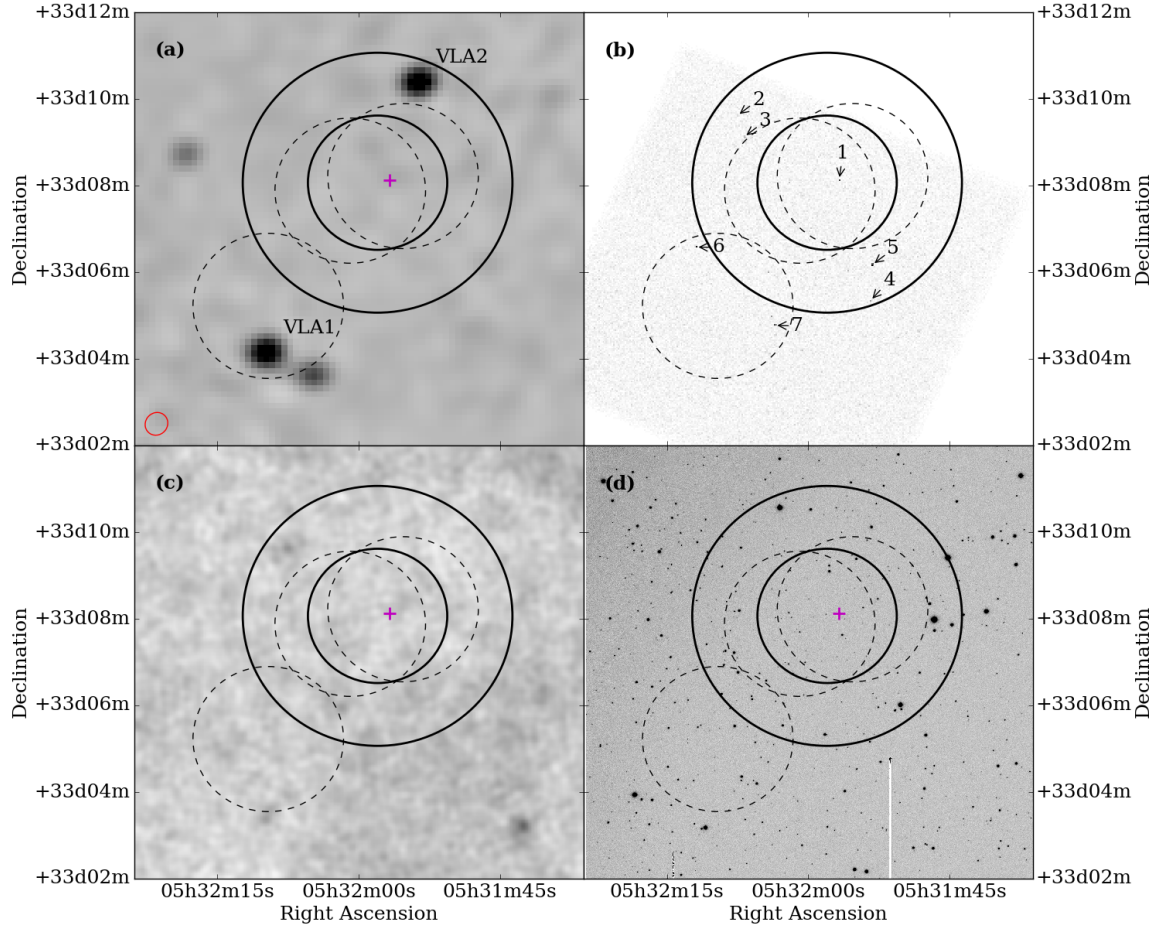


Figure 4. Radio, X-ray, IR, and H α images of the FRB field. In all panels: dashed circles show the ALFA beam locations in which bursts were detected (Spitler et al. 2014, 2016). Their diameters are the 3.4' FWHM of the ALFA beams. The solid circles denote the best estimated radio position with two uncertainty regions shown: the 3.1' FWHM of the L-wide receiver (with which we have detected a burst) and the more conservative 6' diameter region. (a) Jansky VLA 1.6-GHz image of the field of FRB 121102. The red ellipse (lower left) shows the approximate VLA synthesized beam size (31'' \times 36''). Sources labelled “VLA1” and “VLA2” are the sources J053210+3304 and J053153+3310 (Kulkarni et al. 2015, see Section 4.1). (b) *Chandra* image of the field of FRB 121102. The detected X-ray sources are numbered as in Table 4. (c) WISE 22- μ m image from the WISE archive. (d) IPHAS H α image from IPHAS archive. In panels (a), (c), and (d), the magenta cross represents the position of CXOU J053156.7+330807 which is numbered “1” in panel (b) and Table 4.

Table 4
Detected *Chandra* X-ray Sources

No.	Name	RA (J2000) (hh:mm:ss.sss)	Dec (J2000) (dd:mm:ss.ss)	Counts in 1'' circle	Separation ^a (')	IPHAS Counterpart	WISE Counterpart
1	CXOU J053156.7+330807	05:31:56.711	+33:08:07.59	35	0.28	N	Y
2	CXOU J053207.5+330936	05:32:07.534	+33:09:36.87	10	2.5	Y	Y
3	CXOU J053206.8+330907	05:32:06.818	+33:09:07.40	37	2.1	N	N
4	CXOU J053153.4+330520	05:31:53.407	+33:05:20.41	18	2.9	N	N
5	CXOU J053153.2+330610	05:31:53.221	+33:06:10.26	112	2.1	N	N
6	CXOU J053211.9+330635	05:32:11.942	+33:06:35.12	42	3.3	N	N
7	CXOU J053203.5+330446	05:32:03.587	+33:04:46.65	36	3.5	Y	N

^a Angular offset from the average ALFA position of RA=05^h31^m58^s and Dec=+33°08'04" (see Section 2).

the *Chandra* sources (Table 4 and Figure 4b) in the WISE and IPHAS source catalogs. For each *Chandra* source, we looked for sources in the IPHAS catalog that are within $2''$ of the *Chandra* position and for sources within $10''$ from the WISE catalog. In Table 4 we show whether each source has an IPHAS or WISE counterpart. The source CXOU J053207.5+330936 has both an IPHAS and WISE counterpart and is coincident with the star TYC 2407-607-1 (Høg et al. 2000). The source CXOU J053203.5+330446 has an IPHAS optical counterpart ($r' = 15.6$, $i' = 15.0$) but no WISE counterpart (note that this source is outside our conservative uncertainty region). The source CXOU J053156.7+330807, the only source within the 1.4 GHz FWHM region of FRB 121102, does not have an optical counterpart in IPHAS, but does have a WISE counterpart (one of the 9 WISE sources classified as galaxies above).

4.4. Archival High-Energy Observations

An examination of the transient catalogs from *Swift* BAT, *Fermi* GBM, *MAXI*, and *INTEGRAL* reveals that no hard X-ray/soft γ -ray bursts have been reported within $\sim 1^\circ$ of FRB 121102's position. In principle, high-energy counterparts to the radio bursts may be below the significance threshold necessary to trigger a burst alert. To explore this possibility, we retrieved the *Fermi* GBM daily event data from all twelve detectors to check for any enhancement in count rate during the times of the FRB bursts. We find that the event rates within ± 10 s of the radio bursts (after correcting for dispersive delay between radio and gamma-ray arrival times) are fully consistent with that of the persistent GBM background level. The absence of soft γ -ray emission associated with the FRB 121102 radio bursts rules out a bursting magnetar within a few hundred kpc (Younes et al. 2016).

In the *Fermi* LAT 4-year Point Source Catalog (3FGL; Acero et al. 2015) there are no γ -ray sources positionally coincident with FRB 121102. This is confirmed by a binned likelihood analysis, which shows no γ -ray excess at FRB 121102's position that may arise due to a persistent source. This is not surprising, given the Galactic latitude of $b = -0.2^\circ$, where the diffuse γ -ray background is high. On the other hand, if the γ -ray emission is also transient, the source may be evident in the *Fermi* LAT light curve. To this end, we generated exposure-corrected light curves using aperture photometry with a circle of radius 1° binned at 1, 5, 10, and 60-day intervals. None of these exhibit any statistically significant increase in flux, including around the times of the radio detections. In addition, within 1° of FRB 121102, none of the individual γ -rays detected arrive close in time to the radio bursts, after correction for dispersive delay.

5. GALACTIC OR EXTRAGALACTIC?

It is important to consider whether FRB 121102 may be Galactic, despite its DM being three times the maximum Galactic contribution predicted along the line of sight. The source's repetition sheds new light on this question. Here we make use of some of the arguments of Kulkarni et al. (2015), who gave this source considerable thought prior to our discovery of repeat bursts.

Assuming a Galactic contribution of 188 pc cm^{-3} (Cordes & Lazio 2002) to the DM of 559 pc cm^{-3} for

FRB 121102, we take the ‘anomalous’ amount that must be explained to be $\text{DM}' \equiv 559 - 188 = 371 \text{ pc cm}^{-3}$.

This anomalous DM contribution could be explained by an intervening ionized nebula aligned by chance along the line-of-sight, or one in which the source is embedded. As discussed in Kulkarni et al. (2014) and Kulkarni et al. (2015), such a nebula will also necessarily emit and absorb radiation. We now show that, under reasonable assumptions, such emission should have been detected if the source is located within our Galaxy. Here $\text{DM}' = n_e L_{pc}$ for a homogeneous electron distribution and L_{pc} is the putative nebular size in pc. Such a nebula has an emission measure $\text{EM} = \text{DM}'^2 / L_{pc} = 138,000 L_{pc}^{-1} \text{ pc cm}^{-6}$ if one ignores electron density fluctuations in the nebula. If fluctuations are included, EM could be larger by up to a factor of four and if the filling factor ϕ is small, EM could be even larger. In the following, we assume a spherical nebula but address the validity of this assumption at the end.

Assuming a nebular electron temperature of 8000 K , typical for such photoionization, the optical depth to free-free absorption is (e.g. Kulkarni et al. 2014)

$$\tau_{\text{ff}} = 4.4 \times 10^{-7} \text{EM} \left(\frac{T_e}{8000 \text{ K}} \right)^{-1.35} \left(\frac{\nu}{1 \text{ GHz}} \right)^{-2.1}, \quad (2)$$

or

$$\tau_{\text{ff}} = 0.03 L_{pc}^{-1} \left(\frac{T_e}{8000 \text{ K}} \right)^{-1.35} \left(\frac{\nu}{1.4 \text{ GHz}} \right)^{-2.1}, \quad (3)$$

where the frequency normalization has been changed to be the approximate center of the ALFA band.

The highly variable spectra of the source in the ALFA band, as reported by Spitler et al. (2016), indicate that they are intrinsic to the source and suffer little absorption, i.e. $\tau_{\text{ff}} \ll 1$ (see Section 7.1). Equation 3 therefore implies $L_{pc} \gg 0.03 \text{ pc}$. Given that $\text{DM}' = n_e L_{pc}$, this implies an electron density $n_e \ll 12,500 \text{ cm}^{-3}$ and emission measure $\text{EM} = \text{DM}'^2 / L_{pc} \ll 4.6 \times 10^6 \text{ pc cm}^{-6}$. At a fiducial Galactic distance²⁴ of 5 kpc , such a source's angular extent $\theta \gg 1.2''$.

Note that the lack of deviation of the dispersion index from the cold plasma dispersion value of -2 also yields a constraint on source size (Katz 2014). However it is far less constraining than that from the absence of free-free absorption.

In the optically thin regime, the free-free volume emissivity is given by $\epsilon_\nu = 5.4 \times 10^{-39} T_e^{1/2} n_e^2 g \text{ erg cm}^{-3} \text{ s}^{-1} \text{ Hz}^{-1} \text{ sr}^{-1}$ (Rybicki & Lightman 1979) for a pure hydrogen plasma, where g is the Gaunt factor, approximately 5.5 for our case. Note that the above expression is roughly independent of ν in the optically thin regime. Normalizing in temperature and using $n_e = \text{DM}' / L_{pc}$ we have

$$\epsilon_\nu = 4.5 \times 10^{-35} (T_e / 8000 \text{ K})^{1/2} L_{pc}^{-2} \text{ erg cm}^{-3} \text{ s}^{-1} \text{ Hz}^{-1} \text{ sr}^{-1}. \quad (4)$$

²⁴ For a fiducial distance to the source of 5 kpc , the Galactic column would have to be significantly less than the maximum along this line of sight, but this would only strengthen the conclusions that follow, since the electron column of a putative nebula, DM' , would have to be even higher.

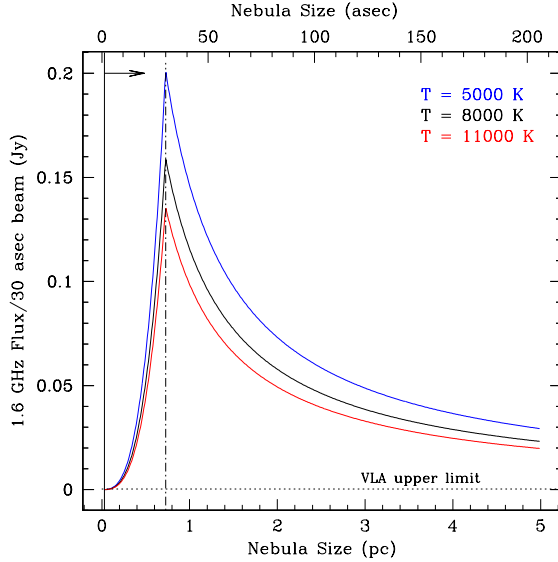


Figure 5. Predicted 1.6-GHz free-free continuum flux per 30'' beam (corresponding to the angular resolution of our VLA observations; Section 4.1) versus assumed size of a putative intervening ionized nebula, in pc (lower horizontal axis), and in arcseconds (upper horizontal axis) for a distance of 5 kpc. The vertical solid line shows the size constraint (lower limit) from the knowledge that the nebula must be optically thin. The vertical dot-dashed line corresponds to the angular resolution of our VLA data. The upper limit on point source flux in our field is shown with a horizontal dotted line and corresponds to 0.3 mJy/beam. Curves for three different assumed plasma temperatures are shown.

To get the luminosity density l in $\text{erg s}^{-1} \text{ Hz}^{-1}$, assuming isotropy, we multiply the above expression by 4π , as well as by the volume of the nebula, $V = (4/3)\pi(L_{cm}/2)^3 \text{ cm}^3$, and then divide l by $4\pi d_{cm}^2$ to get the total source flux density. To compare with observed maps of the region, we must further multiply by $(\theta/\phi_{beam})^2$ for an unresolved source, and by $(\phi_{beam}/\theta)^2$ for a resolved source, where θ is the source angular extent on the sky given L , and ϕ_{beam} is the angular resolution of the map.

As shown in Figure 5, from our VLA upper limit (0.3 mJy/beam in a $\sim 30''$ beam; see Section 4.1) we can rule out any such nebula based on the absence of free-free continuum emission at 20 cm. This is consistent with the conclusion that there is no H II region along the line of sight from the WISE 22- μm map (see Section 4.3 and Anderson et al. 2014).

Moreover, recombination radiation in the form of H α emission would also have to be present for a putative nebula; next we show that the predicted H α flux is ruled out by observations in the IPHAS H α survey of the northern Galactic plane (Drew et al. 2005). As discussed by Kulkarni et al. (2014) and Kulkarni et al. (2015), the H α surface brightness is given by $I = 1.09 \times 10^{-7} \text{ EM erg cm}^{-2} \text{ s}^{-1} \text{ sr}^{-1}$. If we take $\text{EM} = \text{DM}^2/L_{pc}$ and integrate I over the area of the nebula, $\pi\theta^2/4$, the permitted range of L_{pc} implies a predicted H α flux of $1.4 \times 10^{-11} \text{ erg cm}^{-2} \text{ s}^{-1} < f_{H\alpha} < 1.2 \times 10^{-10} \text{ erg cm}^{-2} \text{ s}^{-1}$ or in IPHAS parlance (see Eq. 11 and Appendix D in Kulkarni et al. 2015) $8.0 < ha < 10.4$ for an assumed distance of 5 kpc. Even at a distance of 20 kpc, $ha < 13.4$. This is strongly ruled out given that the IPHAS catalog shows no non-stellar sources in our field (which is encompassed, fortuitously, by the area ex-

amined by Kulkarni et al. 2015) yet contains objects as faint as $ha = 19$ (Kulkarni et al. 2015).

As argued by Kulkarni et al. (2014), a nebula having electron density filling factor $\phi < 1$ only strengthens the constraint on L_{pc} , making the lower limit larger by a factor of $1/\phi$. Also, those authors discussed the possibility of a flash-ionized nebula but predict a flux level comparable to those estimated above, and recombination timescale of years. This is therefore ruled out for FRB 121102. One possibility we cannot absolutely exclude, however, is a greatly elongated nebula with long axis specifically in our direction. However, this seems contrived and highly unlikely. Note that the above conclusions apply even if the Cordes & Lazio (2002) NE2001 model under-predicts the Galactic column along this line-of-sight by as much as a factor of 2.

6. UPDATED PALFA FRB DETECTION RATE

Several studies have noted a possible dependence of the FRB rate on Galactic latitude (e.g. Petroff et al. 2014). One possibility, for an underlying source population that is isotropic, is that foreground effects such as unmodeled Galactic scattering (Burke-Spolaor & Bannister 2014) result in relatively fewer detections near the Galactic plane. Alternatively, Macquart & Johnston (2015) have suggested that the rate of FRBs far out of the plane may be enhanced relative to that in the plane due to diffractive scintillation effects. The PALFA survey is in principle well suited to test these claims by comparing its FRB detection rate with that of higher latitude surveys that also operate at 1.4 GHz. Here we define a FRB as any few-ms radio burst that has DM at least twice the maximum along the line of sight as predicted by the Cordes & Lazio (2002) NE2001 model, and for which the DM excess cannot be explained by any intervening Galactic structure.

To estimate the FRB rate implied by the PALFA survey to date, we make use of the results of the PALFA analysis pipeline described by Lazarus et al. (2015) and run on the Guillimin supercomputer operated by Compute Canada and McGill University. As part of this pipeline PRESTO's routine `single_pulse_search.py` was run on all PALFA data obtained after 2009 March 17 using the Mock spectrometers (see Lazarus et al. 2015, for details). This pipeline's output was subject to the grouping and rating scheme RRATtrap described by Karako-Argaman et al. (2015). In the PALFA analysis pipeline, any beam containing a single pulse having S/N greater than 9.2 was inspected. This threshold S/N applies for all the searched pulse widths, which range from 1 to 150 times the 65.5- μs bin size. To convert this S/N to a flux density, we use the expression given by Cordes & McLaughlin (2003):

$$S_i = \frac{\beta(S/N)_b S_{sys}}{W_i} \sqrt{\frac{W_b}{n_p B}}, \quad (5)$$

where S_i is the intrinsic flux density of the pulse, β is a factor accounting for sensitivity losses due to digitization, $(S/N)_b$ is the measured S/N of the broadened pulse, S_{sys} is the system-equivalent flux density, W_i and W_b are the intrinsic and broadened pulse widths, respectively, n_p is the number of summed polarizations, and B is the bandwidth. Here we adopt $\beta = 1$, $(S/N)_b = 9.2$, $W_i = W_b$,

$n_p = 2$, and $B = 322$ MHz. We consider two cases for S_{sys} : $S_{sys} = 5$ Jy, the field-of-view-averaged system flux in the FWHM of the ALFA beams, and $S_{sys} = 27$ Jy for the full field-of-view of the sidelobe region down to the gain equivalent to that of the Parkes 1.4-GHz beam on-axis. These numbers translate to a sensitivity limit of 57 mJy in the FWHM case and 300 mJy in Parkes-equivalent case.

As of 2015 November 28, PALFA has discovered $N_{FRB} = 1$ (Spitler et al. 2014) while surveying exclusively in the Galactic longitude ranges $30^\circ < l < 75^\circ$ (inner Galaxy) and $174^\circ < l < 205^\circ$ (outer Galaxy) and Galactic latitude range $-5^\circ < b < 5^\circ$.

The FRB rate can be determined using the total sky area surveyed per observation, Θ , and the total time spent observing, T_{obs} . Here we ignore all observations having Galactic longitude $< 40^\circ$ as these include lines of sight for which the 1.4-GHz scattering time is likely to be more than several milliseconds for sources at large distances ($\gtrsim 3$ kpc). Then the rate, R , is given by

$$R = \frac{N_{FRB}}{\Theta \times T_{obs}}, \quad (6)$$

Taking into account beam-dependent gain variations of the ALFA receiver, each pointing covers $\Theta = 0.022$ sq. deg. when considering the FWHM case (i.e. the region having at least half the peak gain of the outer ALFA beams) and $\Theta = 0.105$ sq. deg. when considering the Parkes-equivalent case (Spitler et al. 2014). To determine T_{obs} , we multiply the total number of pointings observed in the PALFA survey between 2009 March 17 and 2015 November 28 by the average integration time per pointing, 233 s. Also, we note that any beam having more than 20% mask fraction due to RFI went unanalyzed by our pipeline; these pointings amount to 0.6% of all beams and are ignored in this calculation. Finally, we make a small correction for time lost due to RFI masking. The average mask fraction for those observations that were analyzed by the pipeline (i.e. those with mask fraction $< 20\%$) was 6%, conservatively estimating that the entire fraction is from masking in time (rather than radio frequency). In this way, we find $T_{obs} = 36.9$ days. Using Equation 6, we therefore find

$$R = 1.4 \times 10^{-5} \text{ FRBs sq. deg}^{-1} \text{ s}^{-1}, \quad (7)$$

or $5.08^{+17.78}_{-4.81} \times 10^4 \text{ FRBs sky}^{-1} \text{ day}^{-1}$

for the FWHM case, i.e. above 57 mJy, and

$$R = 3.0 \times 10^{-6} \text{ FRBs sq. deg}^{-1} \text{ s}^{-1}, \quad (8)$$

or $1.06^{+3.72}_{-1.01} \times 10^4 \text{ FRBs sky}^{-1} \text{ day}^{-1}$

for the Parkes-equivalent case, i.e. above 300 mJy, where we have assumed Poisson statistics to evaluate the quoted 95% confidence range. Note that if we consider only the outer Galaxy beams that PALFA has observed (where scattering is certainly minimal), our upper limits increase by approximately 65% owing to reduced observing time.

Our estimated rate for the combined inner ($l > 40^\circ$) and outer Galaxy survey regions is lower than the event rate estimated by Spitler et al. (2014) because PALFA has observed for longer since the latter calculation was done and Spitler et al. (2014) considered

only the outer Galaxy region. Our number is consistent with the rate derived by Rane et al. (2016), $4.4^{+5.2}_{-3.1} \times 10^3 \text{ FRBs sky}^{-1} \text{ day}^{-1}$ (though note the difference in threshold definition), hence neither confirms nor refutes the claimed dearth in the FRB rate at low Galactic latitudes (Burke-Spolaor & Bannister 2014).

On the other hand, the above estimated PALFA FRB rate is in poor agreement with the prediction of Macquart & Johnston (2015) who assert that PALFA should detect ~ 1 FRB every four days at low Galactic latitudes, based on a model in which diffractive interstellar scintillation (DISS) is responsible for the disparity in event rates of FRBs between high and low Galactic latitudes (Petroff et al. 2014). In the model, an effect associated with Eddington bias enhances the rate of high-latitude FRBs since the expected decorrelation bandwidth for DISS at high latitudes is comparable to the bandwidth. But, at low latitudes, the narrower DISS bandwidth allows only small variations of the flux densities. In order to explain the disparity, Macquart & Johnston (2015) require a steep differential flux density distribution for the FRB population ($p(S_\nu) \propto S_\nu^{-3.4}$ or steeper). This implies a relatively large number of FRBs at low flux densities, hence a higher predicted PALFA event rate, given PALFA's unparalleled raw sensitivity compared to other pulsar surveys. That we have detected only one FRB in ~ 37 days suggests that the difference in FRB rate at high and low latitudes is due primarily to an effect other than that suggested by Macquart & Johnston (2015), such as refractive interstellar scintillation.

7. DISCUSSION

We have presented the discovery of six additional FRB 121102 bursts with GBT and Arecibo as well as multi-wavelength images of the surrounding field.

The detection of FRB 121102 with both Arecibo and GBT rules out a local source of RFI as the origin of the bursts (the telescopes are geographically separated by ~ 2500 km). As previously noted, the detection in only a single pixel of the Arecibo 7-beam ALFA receiver also shows that the bursts must originate beyond Arecibo's Fresnel length of ~ 100 km (Kulkarni et al. 2015; Spitler et al. 2016). In a similar vein, it is also important to note that the consistent sky position of the bursts, to within at least $\sim 6'$, indicates that the source at least approximately follows the sidereal reference frame and has a minimum distance of ~ 1150 AU. Hence, this also rules out the possibility that the bursts could originate from a man-made satellite.

The bursts display extreme spectral variations and an episodic burst rate. We have reiterated, using our new VLA images, as well as archival WISE and IPHAS data, that the source is almost certainly extragalactic, as the high DM cannot be explained by any detected excess dispersive material within our Galaxy. Here we discuss the possible physical causes of the unusual properties of these bursts in the context of an extragalactic origin and compare them to the other currently known FRBs.

7.1. Spectral shape

The 11 bursts discovered in ALFA data presented by Spitler et al. (2016) displayed significant spectral variability. The bursts were observed with both rising and

falling spectra, and some were found with spectra peaking in the band. Overall, the spectral behavior could be described as consisting of a feature with bandwidth comparable to the 322 MHz ALFA band, a feature that varied in peak frequency from burst to burst. It is not clear whether the behavior is caused by a single feature or a broadband spectrum that is strongly modulated at a frequency scale of 100–1000 MHz. The spectral behavior of the GBT bursts presented here in our 2-GHz observations seems to be consistent with what we see at 1.5 GHz, implying that the unusual spectral behavior persists to at least the higher GBT frequency.

We can rule out DISS as the cause of the observed spectral structure on frequency scales $\Delta\nu \sim 600$ MHz at both 1.5 and 2 GHz. The frequency scale expected for DISS differs markedly from what is observed. The NE2001 estimate for the DISS bandwidth is only 57 kHz at 1.5 GHz and 200 kHz at 2 GHz, more than 10^3 times smaller than the observed spectral structure (assuming an extragalactic origin). Unlike for DISS, the scale of the observed structure does not appear at least qualitatively different between 1.5 GHz and 2 GHz. In addition, the DISS time scale estimated by the NE2001 model (Cordes & Lazio 2002) is ~ 4 min at 1.5 GHz²⁵, whereas we see extreme variation in spectral shape between bursts separated by as little as 1 min.

Empirically, we find no evidence for DISS in the burst spectra on *any* frequency scale, provided the source is not nearby. Two effects can generally account for the absence of DISS: either finite source-size smearing of the diffraction pattern which occurs at an angular size of $\gtrsim 1 \mu\text{arcsec}$ at 1.5 GHz, or the DISS bandwidth is too small to be resolved with our channel bandwidth $\Delta\nu_{\text{ch}} = 0.33$ MHz. However, for the source size to be $> 1 \mu\text{arcsec}$, $\Delta\nu_d$ would need to exceed $\Delta\nu_{\text{ch}}$, which is only the case if the source is closer than about 2 kpc (the distance at which the integration of the NE2001 model yields $\Delta\nu_d = \Delta\nu_{\text{ch}}$). Since the source appears to be unavoidably extragalactic, as discussed in Section 5, it must be the case that $\Delta\nu_d \ll \Delta\nu_{\text{ch}}$.

It is also possible that the observed frequency structure is intrinsic to the source. Observations of giant pulses of the Crab pulsar at 1.4 GHz have shown extreme spectral variability with spectral indices ranging from -15 to $+15$ (Karuppusamy et al. 2010). At higher frequencies (5–10 GHz), banded frequency structure has been observed with similar bandwidths to those we observe in FRB 121102 ($\sim 300 - 600$ MHz; Hankins & Eilek 2007). The center frequencies of these Crab giant pulse bands also seem to vary both during the microsecond duration pulses and from pulse to pulse.

7.2. Episodic Behavior

We have now observed FRB 121102 for over 60 hr using radio telescopes, with the majority of observations resulting in non-detections (note, however, that the 60 hr is spread over telescopes with different sensitivities and these observations were performed at several different radio frequencies; see Table 1). Of the 17 bursts found, six

²⁵ The four minute estimate is based on the NE2001 model using an effective velocity of 100 km s^{-1} for changes in the line of sight to the source. However, for an extragalactic source the effective velocity is that of the ISM across the line of sight, which is substantially smaller, leading to a longer DISS time scale.

were found within a 10-min period on 2015 June 2 and an additional four were found in a 20-min period on 2015 November 19. The arrival time distribution of the detected bursts is therefore clearly highly non-Poissonian. We discuss here two possibilities for such variation: propagation effects due to the interstellar medium and variations intrinsic to the source.

DISS is highly unlikely to play any role in the intensity variations of the bursts from FRB 121102. Bandwidth averaging of DISS yields a modulation index (RMS relative to mean intensity) that is only $m_d \sim 1/\sqrt{0.3B/\Delta\nu_d} \sim 2.5\%$ at 1.5 GHz with the ALFA system (bandwidth 322 MHz). The burst amplitudes therefore will be largely unaffected by DISS.

However, refractive interstellar scintillation (RISS) may play an important role in the observed burst intensity variations on weeks to months time scales as its characteristic bandwidth is $\Delta\nu_r \sim \nu \gg B$. Using expressions in Rickett (1990), we estimate the RISS modulation index to be $m_r \sim 0.13$ based on the scaling for a Kolmogorov wavenumber spectrum for the electron density. We note, however, that measured modulation indices are often larger than the Kolmogorov prediction (Rickett & Lyne 1990; Kaspi & Stinebring 1992).

The time scale for RISS is uncertain in this case, and the observed episodic time scales are certainly within the range of these uncertainties. We estimate the characteristic time scale for RISS as follows. The length scales in the spatial intensity patterns of DISS and RISS, l_d and l_r , are related to the Fresnel scale $r_F = \sqrt{\lambda L/2\pi}$ according to $l_r l_d = r_F^2$, where L is the effective distance to the Galactic scattering screen. In the NE2001 model, scattering in the direction of FRB 121102 is dominated by the Perseus spiral arm at $L \sim 2$ kpc, giving $r_F \sim 10^{11}$ cm. The diffraction length scale is related to the DISS bandwidth as $l_d \sim \lambda \sqrt{d \Delta\nu_d / 4\pi c}$ (Eq. 9 of Cordes & Rickett 1998) from which we estimate $l_r \sim 4 \times 10^{13}$ cm. The corresponding time scale for RISS depends on the characteristic velocity for motion of the line of sight across the Galactic plasma. Using a nominal velocity of 100 km s^{-1} , we obtain $\Delta t_r \sim 40$ days. However, it is not clear what velocity to use because, unlike pulsars, the source motion is not expected to contribute. If the motions are only from Galactic rotation with a flat rotation curve, the scattering medium and the Sun move together with zero relative velocity. However, non-circular motions, including the solar system's velocity relative to the local standard of rest ($\sim 20 \text{ km s}^{-1}$) and the Earth's orbital velocity, will contribute a total of a few tens of km s^{-1} yielding an RISS time scale longer than 40 days. Given the uncertainties in estimating RISS time scales, it is possible that Δt_r ranges from tens of days to 100 days or more at 1.5 GHz. RISS times scale with frequency as $\Delta t_r \propto \nu^{-2.2}$, so higher frequencies vary more rapidly.

Although variability intrinsic to the source appears to dominate on minutes to hours timescales, RISS could be important for intensity variations on timescales of weeks to months. If we use $m_r = 0.13$ (allowing for the modulation index to be larger than predicted by a factor of 2) at 1.5 GHz and consider $\pm 2m_r$ variations, the maximum and minimum range of the RISS modulation is $g_{r,\text{max}}/g_{r,\text{min}} = 1.7$. If the burst amplitude

distribution is a power law $\propto S^{-\alpha}$, as seen in the Crab pulsar's giant pulses (for which $2.3 \lesssim \alpha \lesssim 3.5$; e.g. [Mickaliger et al. 2012](#)), RISS will cause the apparent burst rate above a detection threshold to vary by an amount $(g_{r,\max}/g_{r,\min})^{\alpha-1} \sim 2 - 4$ for $\alpha = 2.3$ to 3.5 . But note again that modulation indices have been observed to be higher than predicted, so the burst-rate variation could be still higher (e.g. for $m_r = 0.4$, $(g_{r,\max}/g_{r,\min})^{\alpha-1} \sim 20 - 200$). Keeping in mind these uncertainties, it is clear that RISS could cause large variations in the observed burst rate. This issue is being considered in detail in a separate article (Cordes et al., in prep).

For intrinsic phenomena that might cause the episodic behavior, we look at examples from pulsars within our Galaxy, as supergiant pulses from pulsars and magnetars ([Cordes & Wasserman 2016](#); [Pen & Connor 2015](#)) are a viable model for repeating bursts. First, the time separations in Crab giant pulses do not show a deviation from a random process ([Lundgren et al. 1995](#)). However, a subset of young Galactic pulsars display a phenomenon known as nulling in which they emit pulses only a fraction of the time. The nulling fractions of these pulsars can be quite high, the most extreme emitting pulses $<5\%$ of the time ([Wang et al. 2007](#)). Some Rotating Radio Transients (RRATs), a class of Galactic radio pulsar that emit infrequent, bright millisecond duration radio pulses, also show episodic behavior in their pulses ([Keane et al. 2010](#)). It is therefore possible that, if the bursts from FRB 121102 originate from a rotating neutron star, a similar process is causing the episodic behavior in FRB 121102.

Another example of young neutron stars in our Galaxy emitting bursts in episodes are X-ray bursts from magnetars. Magnetar X-ray bursts have time scales from milliseconds to seconds and are emitted in clusters during periods of outburst (e.g. [Görgüç et al. 2001](#); [Gavriil et al. 2004](#); [Scholz & Kaspi 2011](#)). [Lyutikov \(2002\)](#) suggests that these X-ray bursts may have accompanying radio emission. To date, no radio counterpart to a magnetar X-ray burst has been observed (e.g. [Tendulkar et al. 2016](#)), but the possibility remains that it is what we are observing for FRB 121102.

7.3. Comparison to other FRBs

Here we compare some of the properties of FRB 121102's 12 Arecibo-detected bursts against equivalent properties from the 15 FRBs so far reported from Parkes observations (see FRBCAT). We limit ourselves to the 1.4- GHz detected bursts, so that we are comparing bursts from the same frequency range to each other.

Three of the Parkes FRBs, including the first reported ([Lorimer et al. 2007](#)), were detected with an analog filterbank system, with 3-MHz-wide frequency channels. These cause an intra-channel dispersion smearing time, Δt_{DM} , 8 times larger than the equivalent for the other Parkes FRBs, detected with the BPSR backend (with 0.39 MHz channel width), or for the ALFA observations of FRB 121102 (0.34 MHz width).

The 12 Arecibo FRB 121102 pulses have measured widths spanning 3–9 ms ([Spitler et al. 2016](#)). Given that Δt_{DM} for the bursts detected with ALFA is 0.7 ms and zero for the PUPPI-detected burst (as it was coherently dispersed), and that no scattering tail is observed in the pulses, the observed widths must be the intrinsic width

of the emission.

Two of the 15 Parkes FRBs have two-component profiles (as do some of the FRB 121102 pulses, although their shape is varied and not obviously comparable to those of the Parkes events), and we neglect them here. The observed widths of the remaining 13 FRBs span 0.6–9 ms, apparently comparable to the widths of FRB 121102 bursts. However, at least two (see [Thornton et al. 2013](#); [Ravi et al. 2015](#)), and possibly four (see [Lorimer et al. 2007](#); [Petroff et al. 2015a](#)) of the Parkes FRBs display significant evidence of multi-path propagation/scattering, which can make their observed widths larger than their intrinsic widths. In addition, two Parkes FRBs have $\Delta t_{\text{DM}} = 7$ ms, comparable to their observed widths ([Keane et al. 2011](#); [Burke-Spolaor & Bannister 2014](#)).

After accounting for all instrumental and measurable propagation effects, none of the 13 Parkes single-component FRBs is wider than ~ 3 ms. Indeed, several of the Parkes FRBs are temporally unresolved: e.g., FRB 130628 has an observed width of 0.6 ms and $\Delta t_{\text{DM}} \sim 0.6$ ms; ([Champion et al. 2015](#)).

In summary, it appears that the intrinsic widths of the 12 FRB 121102 bursts from Arecibo (3–9 ms) are significantly longer than the intrinsic widths of the 13 single-component Parkes FRBs ($\lesssim 3$ ms).

We can also compare the spectra of the FRB 121102 bursts with those of Parkes FRBs. The collection of FRB 121102 bursts has spectra that in some cases can be approximated by power laws with indices spanning $-10 < \alpha < +14$. In some instances, the spectral behavior is more complex and cannot be approximated by a power law ([Spitler et al. 2016](#), Fig. 2).

Only nine of the 15 Parkes FRBs have sufficiently well described spectral properties to allow at least qualitative judgements on their spectra. In most such cases, the original references do not provide quantitative spectral information, but a “waterfall” plot (showing a grayscale of the pulse flux density as a function of observing frequency, as in Fig. 2) is available with sufficient S/N in these nine cases. Note that the waterfall plots for FRBs 090625, 110703, and 130729 are not published in the refereed literature but are available at FRBCAT.

For seven of the Parkes FRBs, within the available S/N, the spectrum appears consistent with showing roughly monotonic flux density frequency evolution and qualitatively consistent with mildly negative spectral indices as for ordinary radio pulsars (e.g. [Manchester & Taylor 1977](#)). A closer look shows possible departures from this general trend (e.g., for FRB 110220; see Figure S4 of [Thornton et al. 2013](#)), but likely propagation effects need to be accounted for when considering this issue in detail. Two Parkes FRBs have published spectral indices: [Ravi et al. \(2015\)](#) report a marginally inverted spectrum for FRB 131104, with $\alpha = 0.3 \pm 0.9$, but caution that this value could be different depending on the true position of the FRB within the telescope beam pattern. [Keane et al. \(2016\)](#) report $\alpha = 1.3 \pm 0.5$ for FRB 150418, but a similar caveat applies in that they assume the position of the possibly coincident variable source detected in a galaxy within the Parkes beam pattern (but see [Williams & Berger 2016](#); [Vedantham et al. 2016](#)).

In summary, the largely qualitative spectra inferred for nine Parkes FRBs may show in a few cases departure

from standard pulsar-like spectra, but even in the best such counter-examples, a possibly uncertain FRB position renders such conclusions tentative. In contrast, the collection of Arecibo spectra from FRB 121102 bursts displays intrinsic variability that includes examples with very positive and very negative spectral indices, not represented in the Parkes collection.

Two other useful quantities to compare are the observed peak flux density S_{peak} and fluence F of the various FRBs. Arecibo detections of FRB 121102 have $0.02 < S_{\text{peak}} < 0.3 \text{ Jy}$ and $0.1 < F < 1 \text{ Jy ms}$. For the most part, the Parkes FRBs have S_{peak} and F an order of magnitude larger than the Arecibo FRB 121102 values: $0.2\text{--}2.2 \text{ Jy}$ and $1\text{--}7 \text{ Jy ms}$, respectively. The one exception is FRB 010724 (Lorimer et al. 2007), which is yet another order of magnitude brighter ($S_{\text{peak}} \sim 30 \text{ Jy}$ and $F \sim 150 \text{ Jy ms}$).

The Arecibo ALFA system, used to detect the FRB 121102 bursts near 1.4 GHz, is ~ 10 times more sensitive than the multibeam receiver system used to detect all Parkes FRBs. It is thus not surprising that the faintest Arecibo FRB detections have flux densities an order of magnitude smaller than those of the faintest Parkes FRBs. That the strongest FRB 121102 detections are one to two orders of magnitude below the strongest Parkes FRB detections could reflect a luminosity distribution favoring fainter bursts. Indeed, there are more FRB 121102 bursts near the Arecibo detection limit than high S/N bursts. The lack of repeated burst detections to date from Parkes FRBs might be due to the Parkes telescope's lower sensitivity not probing as deeply into the flux density distribution for putative repeating FRBs.

In any case, it is possible that with more time on source, some of the Parkes FRBs will be found to be repeating. Based on current observations, however, we cannot exclude the possibility that Parkes FRBs represent a non-repeating population, and thus are fundamentally different from FRB 121102. The differing pulse widths and spectra as discussed above may provide modest support for this idea.

8. SUMMARY AND CONCLUSIONS

Our discovery of repeating bursts from FRB 121102 shows that, for at least one source, the origin of the bursts cannot be cataclysmic, and further, must be able to repeat on short ($\lesssim 1 \text{ min}$) time scales. Whether FRB 121102 is a unique object in the currently known sample of FRBs, or all FRBs are capable of repeating, its characterization is extremely important to understanding fast extragalactic radio transients.

Here, we have shown that bursts from FRB 121102 are detected at 2 GHz (with GBT) as well as 1.4 GHz (with Arecibo). The spectra of those bursts are also not well described by a typical power law and vary significantly from burst to burst. These variations cannot be due to diffractive interstellar scintillation and are therefore likely intrinsic. As noted by Spitler et al. (2016) the spectral variations are somewhat reminiscent of those sometimes seen in the Crab pulsar. The episodic burst rate that we observe from FRB 121102 could be explained by modulation by refractive interstellar scintillation, but intrinsic explanations based on phenomena displayed by Galactic pulsars and magnetars could also work.

We have also presented observations of the field from

the VLA, and the *Chandra* and *Swift* X-ray telescopes, as well as archival optical/IR observations from WISE and IPHAS. None of these observations shows an obvious counterpart to FRB 121102. Further, from these observations, we have placed a limit on the existence of a Galactic nebula that provides the excess dispersion. We find it extremely unlikely that FRB 121102 is Galactic, as any nebula that could provide the observed dispersion should be visible in VLA, WISE, and/or IPHAS observations.

The nearly certain extragalactic distance and repeating nature of FRB 121102 lead us to favor an origin for the bursts that invokes a young extragalactic neutron star. Super-giant pulses from young pulsars or magnetars (Cordes & Wasserman 2016; Pen & Connor 2015) or radio counterparts to magnetar X-ray bursts (Lyutikov 2002; Popov & Postnov 2013; Katz 2015) remain plausible models. As young neutron stars are expected to be embedded in star-forming regions as well as supernova remnants, i.e. regions composed of a high amount of dispersing plasma, we expect a large host contribution to the excess DM. This could lead to a smaller distance for FRB 121102 than the $\sim 1 \text{ Gpc}$ implied if the majority of the dispersion comes from the IGM (Spitler et al. 2014). This would reduce the seemingly extreme luminosities required for these distant bursts.

However, the distance will remain uncertain until a host galaxy for FRB 121102 can be identified. Such an identification could occur either by detecting radio bursts with interferometry in order to achieve the $\sim 1''$ localization required, or by finding correlated variability at other wavelengths (e.g. coincident X-ray bursts). Such efforts are currently underway.

Finally, we have updated the observed FRB rate for the PALFA survey given the longer baseline of observations since that reported by Spitler et al. (2014) and find that we can still neither confirm nor refute the claimed Galactic latitude dependence of the observed FRB rate. However, our revised rate is now in disagreement with the expectations of the diffractive interstellar scintillation model of Macquart & Johnston (2015) that attempts to account for the latitude dependence.

We thank A. Lyne for coordinating the Lovell telescope observations and P. Demorest for help with the VLA observations.

L.G.S., J.W.T.H., C.G.B., and J.v.L. gratefully acknowledge support from the European Research Council under the European Unions Seventh Framework Programme (FP/2007-2013)/ERC Grant Agreement nos. 279702 (L.G.S.), 337062 (J.W.T.H., C.G.B.), and 617199 (J.v.L.). J.W.T.H. is an NWO Vidi Fellow. V.M.K. holds the Lorne Trottier and a Canada Research Chair and receives support from an NSERC Discovery Grant and Accelerator Supplement, from a R. Howard Webster Foundation Fellowship from the Canadian Institute for Advanced Research (CIFAR), and from the FRQNT Centre de Recherche en Astrophysique du Québec. J.S.D. was supported by the NASA Fermi Guest Investigator program and the Chief of Naval Research. Pulsar research at UBC is supported by an NSERC Discovery Grant and by CIFAR.

We thank the staff of the Arecibo Observatory, and in particular A. Venkataraman, H. Hernandez, P. Perillat

and J. Schmelz, for their continued support and dedication to enabling observations like those presented here.

The Arecibo Observatory is operated by SRI International under a cooperative agreement with the National Science Foundation (AST-1100968), and in alliance with Ana G. Méndez-Universidad Metropolitana, and the Universities Space Research Association.

The National Radio Astronomy Observatory is a facility of the National Science Foundation operated under cooperative agreement by Associated Universities, Inc.

The scientific results reported in this article are based in part on observations made by the Chandra X-ray Observatory.

This publication makes use of data products from the Wide-field Infrared Survey Explorer, which is a joint project of the University of California, Los Angeles, and the Jet Propulsion Laboratory/California Institute of Technology, funded by the National Aeronautics and Space Administration.

This paper makes use of data obtained as part of the INT Photometric H α Survey of the Northern Galactic Plane (IPHAS) carried out at the Isaac Newton Telescope (INT). The INT is operated on the island of La Palma by the Isaac Newton Group in the Spanish Observatorio del Roque de los Muchachos of the Instituto de Astrofísica de Canarias. All IPHAS data are processed by the Cambridge Astronomical Survey Unit, at the Institute of Astronomy in Cambridge. The band-merged DR2 catalogue was assembled at the Centre for Astrophysics Research, University of Hertfordshire, supported by STFC grant ST/J001333/1.

This research has made use of the NASA/IPAC Infrared Science Archive, which is operated by the Jet Propulsion Laboratory, California Institute of Technology, under contract with the National Aeronautics and Space Administration.

These data were processed using the McGill University High Performance Computing Centre operated by Compute Canada and Calcul Québec.

REFERENCES

Acero, F., Ackermann, M., Ajello, M., et al. 2015, *ApJS*, 218, 23

Anderson, L. D., Bania, T. M., Balser, D. S., et al. 2014, 212, 1

Barentsen, G., Farnhill, H. J., Drew, J. E., et al. 2014, *MNRAS*, 444, 3230

Burke-Spolaor, S., Bailes, M., Ekers, R., Macquart, J.-P., & Crawford, III, F. 2011, *ApJ*, 727, 18

Burke-Spolaor, S., & Bannister, K. W. 2014, *ApJ*, 792, 19

Burrows, D. N., Hill, J. E., Nousek, J. A., et al. 2005, *Space Sci. Rev.*, 120, 165

Champion, D. J., Petroff, E., Kramer, M., et al. 2015, *MNRAS*, submitted

Condon, J. J., Cotton, W. D., Greisen, E. W., et al. 1998, *AJ*, 115, 1693

Cordes, J. M., & Lazio, T. J. W. 2002, *astro-ph/0207156*

Cordes, J. M., & McLaughlin, M. A. 2003, *ApJ*, 596, 1142

Cordes, J. M., & Rickett, B. J. 1998, *ApJ*, 507, 846

Cordes, J. M., & Wasserman, I. 2016, *MNRAS*, 457, 232

Cordes, J. M., Freire, P. C. C., Lorimer, D. R., et al. 2006, *ApJ*, 637, 446

Cutri, R. M., & et al. 2013, *VizieR Online Data Catalog*, 2328

Drew, J. E., Greimel, R., Irwin, M. J., et al. 2005, *MNRAS*, 362, 753

Eatough, R. P., Keane, E. F., & Lyne, A. G. 2009, *MNRAS*, 395, 410

Falcke, H., & Rezzolla, L. 2014, *A&A*, 562, A137

Gavriil, F. P., Kaspi, V. M., & Woods, P. M. 2004, *ApJ*, 607, 959

Gögüs, E., Kouveliotou, C., Woods, P. M., et al. 2001, *ApJ*, 558, 228

Hankins, T. H., & Eilek, J. A. 2007, *ApJ*, 670, 693

Hassall, T. E., Stappers, B. W., Hessels, J. W. T., et al. 2012, *A&A*, 543, A66

He, C., Ng, C.-Y., & Kaspi, V. M. 2013, *ApJ*, 768, 64

Hobbs, G. M., Edwards, R. T., & Manchester, R. N. 2006, *MNRAS*, 369, 655

Høg, E., Fabricius, C., Makarov, V. V., et al. 2000, *A&A*, 355, L27

Kalberla, P. M. W., Burton, W. B., Hartmann, D., et al. 2005, *A&A*, 440, 775

Karako-Argaman, C., Kaspi, V. M., Lynch, R. S., et al. 2015, *ApJ*, 809, 67

Karuppusamy, R., Stappers, B. W., & van Straten, W. 2010, *A&A*, 515, A36

Kashiyama, K., Ioka, K., & Mészáros, P. 2013, *ApJ*, 776, L39

Kaspi, V. M., & Stinebring, D. R. 1992, *ApJ*, 392, 530

Katz, J. I. 2014, *ArXiv e-prints*, arXiv:1409.5766

—. 2015, *ArXiv e-prints*, arXiv:1512.04503

Keane, E. F., Kramer, M., Lyne, A. G., Stappers, B. W., & McLaughlin, M. A. 2011, *MNRAS*, 415, 3065

Keane, E. F., Ludovici, D. A., Eatough, R. P., et al. 2010, *MNRAS*, 401, 1057

Keane, E. F., Johnston, S., Bhandari, S., et al. 2016, *Nature*, 530, 453

Kondratiev, V. I., McLaughlin, M. A., Lorimer, D. R., et al. 2009, *ApJ*, 702, 692

Kulkarni, S. R., Ofek, E. O., & Neill, J. D. 2015, *ArXiv e-prints*, arXiv:1511.09137

Kulkarni, S. R., Ofek, E. O., Neill, J. D., Zheng, Z., & Juric, M. 2014, *ApJ*, 797, 70

Law, C. J., Bower, G. C., Burke-Spolaor, S., et al. 2015, *ApJ*, 807, 16

Lazarus, P., Brazier, A., Hessels, J. W. T., et al. 2015, *ApJ*, in press

Lorimer, D. R., Bailes, M., McLaughlin, M. A., Narkevic, D. J., & Crawford, F. 2007, *Science*, 318, 777

Lorimer, D. R. and Kramer, M. 2005, *Handbook of Pulsar Astronomy* (Cambridge University Press)

Lundgren, S. C., Cordes, J. M., Ulmer, M., et al. 1995, *ApJ*, 453, 433

Lyutikov, M. 2002, *ApJ*, 580, L65

Macquart, J.-P., & Johnston, S. 2015, *MNRAS*, 451, 3278

Manchester, R. N., & Taylor, J. H. 1977, *Pulsars* (San Francisco: Freeman)

Masui, K., Lin, H.-H., Sievers, J., et al. 2015, *Nature*, 528, 523

McMullin, J. P., Waters, B., Schiebel, D., et al. 2007, in *Astronomical Society of the Pacific Conference Series*, Vol. 376, *Astronomical Data Analysis Software and Systems XVI*, ed. R. A. Shaw, F. Hill, & D. J. Bell, 127

Mickaliger, M. B., McLaughlin, M. A., Lorimer, D. R., et al. 2012, *ApJ*, 760, 64

Nikutta, R., Hunt-Walker, N., Nenkova, M., Ivezić, Ž., & Elitzur, M. 2014, *MNRAS*, 442, 3361

Ofek, E. O., Frail, D. A., Breslauer, B., et al. 2011, *ApJ*, 740, 65

Pen, U.-L., & Connor, L. 2015, *ApJ*, 807, 179

Petroff, E., van Straten, W., Johnston, S., et al. 2014, *ApJ*, 789, L26

Petroff, E., Bailes, M., Barr, E. D., et al. 2015a, *MNRAS*, 447, 246

Petroff, E., Johnston, S., Keane, E. F., et al. 2015b, *MNRAS*, 454, 457

Petroff, E., Keane, E. F., Barr, E. D., et al. 2015c, *MNRAS*, 451, 3933

Petroff, E., Barr, E. D., Jameson, A., et al. 2016, *Proc. Astr. Soc. Aust.*, submitted; arXiv:1601.03547

Popov, S. B., & Postnov, K. A. 2013, *ArXiv e-prints*, arXiv:1307.4924

Rane, A., Lorimer, D. R., Bates, S. D., et al. 2016, *MNRAS*, 455, 2207

Ransom, S. M. 2001, PhD thesis, Harvard University

Rau, U., & Cornwell, T. J. 2011, *A&A*, 532, A71

Ravi, V., Shannon, R. M., & Jameson, A. 2015, *ApJ*, 799, L5

Rickett, B. J. 1990, *Ann. Rev. Astr. Ap.*, 28, 561

Rickett, B. J., & Lyne, A. G. 1990, *MNRAS*, 244, 68

Rybicki, G. B., & Lightman, A. P. 1979, *Radiative Processes in Astrophysics* (New York: Wiley)

Scholz, P., & Kaspi, V. M. 2011, *ApJ*, 739, 94

Schwab, F. R. 1984, AJ, 89, 1076

Spitler, L. G., Cordes, J. M., Hessels, J. W. T., et al. 2014, ApJ, 790, 101

Spitler, L. G., Scholz, P., Hessels, J. W. T., et al. 2016, Nature, 531, 202

Staelin, D. H. 1969, Proc. I. E. E. E., 57, 724

Tendulkar, S. P., Kaspi, V. M., & Patel, C. 2016, ArXiv e-prints, arXiv:1602.02188

Thornton, D., Stappers, B., Bailes, M., et al. 2013, Science, 341, 53

Vedantham, H. K., Ravi, V., Mooley, K., et al. 2016, ArXiv e-prints, arXiv:1603.04421

Wang, N., Manchester, R. N., & Johnston, S. 2007, MNRAS, 377, 1383

Williams, P. K. G., & Berger, E. 2016, ArXiv e-prints, arXiv:1602.08434

Wright, E. L., Eisenhardt, P. R. M., Mainzer, A. K., et al. 2010, AJ, 140, 1868

Younes, G., Kouveliotou, C., Huppenkothen, D., et al. 2016, The Astronomer's Telegram, 8781